FLOW PAST A SQUARE CYLINDER: TEST CASE LES2

PETER R. VOKE
Department of Mechanical Engineering
The University of Surrey, Guildford GU2 5XH, UK

Abstract. A series of large-eddy simulations of flow past a square cylinder at $Re = 21400$ have been conducted by seven groups of researchers. A comparative report is presented of the time-average results with a view to establishing any clear advantage of particular subgrid scale modelling approaches, wall treatments, and numerical methods.

1. Background and Specification

The flow past a square cylinder at a Reynolds number of 21400 based on upstream velocity and cylinder side dimension was studied experimentally by Lyn and Rodi (1994) and Lyn *et al.* (1995). The flow is interesting as a test case for LES since it involves semi-coherent shedding of vortices from the cylinder, which is mounted transverse to the flow (Figure 1), breaking down into turbulence. It was selected by W. Rodi and J. Ferziger as a test case for a workshop held at Rottach-Egern, Germany in June 1995, reported by Rodi *et al.* (1996). The same flow was adopted at the First ERCOFTAC Workshop on Direct and Large-Eddy Simulation in March 1994 as test case LES2 to be studied for the Second Workshop reported here.

Since the flow involves coherent shedding of vortices from the cylinder, both the experimental data of Lyn *et al.* (1995) and the computations submitted to the Rodi-Ferziger workshop involved detailed phase averages at various phases through the shedding cycle. The phase averages constitute a large mass of data, and do not appear to add greatly to an understanding of the advantages and disadvantages of the various LES techniques (subgrid and wall models, resolution effects, etc.) over and above that provided by time-averaged data. In the present exercise, it was specified that only time-averaged data should be submitted for comparison.

J.-P. Chollet et al. (eds.), Direct and Large-Eddy Simulation II, 355-373.

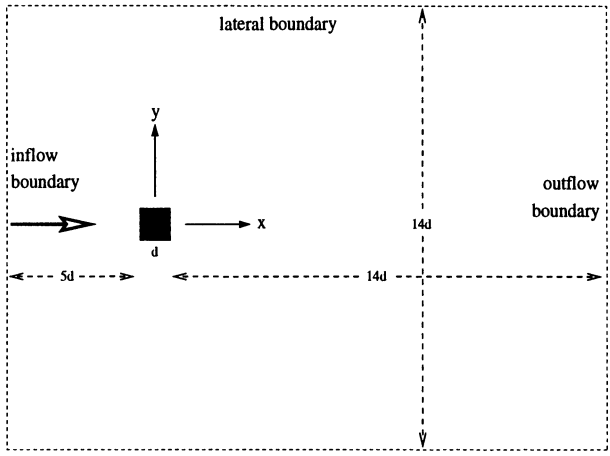

Figure 1. Geometry of the simulations.

2. Contributions to the Test Case

Seven groups have taken part in the test case exercise, though several of these have conducted more extended investigations by varying several aspects or parameters in their simulations, and have therefore submitted more than one dataset. The groups and datasets are as follows: Universität Karlsruhe (datasets UK1 to UK3); University of Groningen (GRO); University of Illinois (UOI); Institute of Technology, Niigata and University of Tokyo (NT1 to NT7); University of Tokyo Institute of Industrial Science (IS1 to IS3); Science University of Tokyo (ST2 to ST5); and the Tokyo Institute of Technology (TIT). This exercise is a continuation of that of Rodi and Ferziger, since all groups except GRO were participants in the Rottach-Egern workshop. The details of the simulations resulting in each of the datasets is laid out in Table 1. Here and elsewhere all distances are normalised by the cylinder dimension d and velocities by the upstream velocity U_0.

The parameters given are: N_x, N_y, N_z, meshes in streamwise, normal and span directions; L_x, the domain length downstream from the cylinder centre to the ouflow plane; Δt, time step in terms of d/U_0; T/T_s, the statistical sampling time in the simulation divided by the shedding period T_s (i.e. the number of cycles over which samples were taken, excluding any startup or conditioning run time); Δ_w, the mesh dimension adjacent and normal to the cylinder surface, in terms of d; b.c. is the type of boundary condition applied at the wall of the cylinder.

Certain computational conditions were specified or suggested for the test case, notably the domain dimensions of $20d \times 14d \times 4d$. (In fact the groups used a variety of streamwise dimensions for their computational do-

TABLE 1. Simulations

set	N_x	N_y	N_z	L_x	$10^3\Delta t$	T/T_s	Δ_w	b.c.	model
UK1	109	105	20	14	1	13.5	0.02	power	$C_s = 0.1$
UK2	146	146	20	14	1	8.3	0.01	power	$C_s = 0.1$
UK3	146	146	20	14	1	12.5	0.01	no-slip	$C_s = 0.1$
GRO	280	210	64	20	1	3	0.005	no-slip	none
NT1-5	104	68	10	14.5	1	8-2	0.022	power	varied*
NT6	107	103	14	14.5	1	2	0.02	power	$C_s = 0.1$
NT7	140	103	32	14.5	1	8	0.02	power	LDMM
UOI	192	160	48	14	2	11	0.01	no-slip	dynamic
IS1	82	63	16	21	2	13	0.04	no-slip	$C_s = 0.13$
IS2	82	63	32	21	2	13	0.04	no-slip	$C_s = 0.13$
IS3	112	104	32	20	2	6.7	0.02	no-slip	dyn. mix.
TIT	121	113	127*	10	1	5	0.005*	no-slip	dynamic
ST2	109	78	20	7.7	0.5	16	0.024	no-slip	$C_s = 0.1$
ST3	125	78	20	11	0.5	15	0.024	no-slip	numerical
ST4	107	103	20	15	0.5	12.5	0.017	no-slip	$C_s = 0.1$
ST5	107	103	20	15	0.5	14.5	0.017	no-slip	$C_s = 0.1$

* Varies: see text.

mains downstream of the cylinder, but this variation does not appear to have affected the results in any obvious way.) This and other suggestions were made on the basis of experience from the Rottach-Egern workshop results; in fact one simulation from that meeting, the submission UKAHY1 from the University of Karlsruhe, was laid down as a baseline configuration for test case LES2, with the contributing groups encouraged to investigate variations and improvements of that computation. Nevertheless the specific numerical methods, subgrid-scale and wall models, mesh concentrations and stretching, boundary conditions and computational efficiency vary considerably in this exercise; we shall therefore now briefly summarise the key aspects of each simulation.

The Karlsruhe group provided the baseline computation UK1 which is identical to UKAHY1 of the Rottach-Egern workshop. UK2 is also included, which is essentially the same as UKAHY2 of the previous workshop, and has higher streamwise and lateral meshing than UK1 to allow a halving of the dimensions of the wall-adjacent meshes. Both UK1 and UK2 use the linear/one-seventh power law artificial boundary condition of Werner and Wengle (1993). The third computation UK3 is new, but differs from UK2 only in applying the no-slip boundary condition on the cylinder surface and in the sampling time which was 50% greater. The code

used is non-staggered (cell-centred) with second-order central differencing and a standard explicit second-order time advancement and pressure correction scheme. The Smagorinsky model was used in all runs, with Van Driest damping functions close to the solid walls. UK3 required 10 hours per shedding cycle on a SNI (Fujitsu) S600/20.

The Groningen group (GRO) used a fourth-order finite-volume method which is detailed by Verstappen amd Veldman (1997) in this volume. Their grid is stretched using a sinh function, the ratio of the largest to the smallest grid being approximately 200 in x and 100 in y. Standard inflow conditions, $u = 1, v = 0, w = 0$, were imposed at $x = -7.0$. Derivative outflow boundary conditions were imposed, $d^2v/dx^2 = 0, d^2w/dx^2 = 0$ and dp/dx approximately zero, its value being determined at each time-step such that the mass inflow equalled the mass outflow. The outflow boundary was located beyond a buffer zone extending from $x = 15$ to 20, in which the Reynolds number was decreased. There was no subgrid model. Samples were taken every time step over three shedding cycles following a startup period of flow conditioning. The computation required 40 hours per shedding cycle on a Cray J916.

The group from the University of Illinois (UOI) performed six simulations as part of their study, of which the fourth is considered the most accurate and is included in this exercise. Further details of these simulations are given by Wang and Vanka (1996), and for the case included here (Wang and Vanka, 1997) later in this volume. The resolution in the spanwise direction is improved by reducing the spanwise domain dimension to πd and using 48 cells. The inflow boundary conditions were standard, the outflow was a convective condition using a convection velocity of 0.7, but the lateral boundaries were moved further away so that the predicted C_D had to be corrected for the different blockage; it is not known what other effects this different blockage may have had. The numerical scheme for the run utilised fifth-order upwind differencing for the convection terms and the fourth-order central scheme for other terms. A dynamic procedure based on the Smagorinsky model was used, stabilised by span averaging and bounding the total viscosity below by zero viscosity. The work was performed on a Thinking Machines CM-5.

The group co-operating between Niigata and Tokyo performed a high resolution simulation NT7 which will be included fully in the subsequent analysis, together with a series of six other test simulations with lower spanwise meshing (10 meshes) and box size ($2d$ instead of $4d$) and also with a very short sampling time (two shedding cycles out of a total run time of 4 cycles in each case, apart from NT1 where $T = 8T_s$). NT6 was slightly different; here the mesh of the baseline solution UKAHY1 from the Rottach-Egern workshop was closely reproduced, though the statistics

were again gathered over two cycles. Since the implications of some of these supporting studies are of interest, the main features of the runs are summarised in Table 2. It is assumed that statistics gathered over two cycles can give no more than an indication of trends.

TABLE 2. Test Simulations NT1 to NT6

set	Feature(s)
NT1	Smagorinsky model with $C_s = 0.13$ and Van Driest damping function
NT2	Dynamic Smagorinsky model; C bounded by zero
NT3	Dynamic mixed model; C bounded below by zero
NT4	Lagrangian dynamic mixed model
NT5	As NT4 but on a staggered Cartesian grid
NT6	Mesh and domain as UKAHY1, ($107 \times 103 \times 14$, domain width $4d$) Smagorinsky model with C_s=0.1 and damping function

Most of the tests used collocated (centered) meshing. NT5 and NT7 used staggered meshing. The inflow and lateral boundary conditions were standard, the outflow convective, and the cylinder walls were subject to the boundary condition of Werner and Wengle (1993) in which a linear subayer is matched to a 1/7 power-law region above. In fact the wall-normal resolution of these simulations was in all cases not notably inferior to that of the other groups, and it is found that the linear law was being used in most regions of the upper and lower surface of the cylinder, exept near the corners. The numerical methods were second-order central differencing in all cases, and time advancement was by Adams-Bashforth for the convection terms and Crank-Nicolson for others. The tests that used the Smagorinsky model employed wall damping functions, $f = 1 - \exp(-y^+/25)$ for NT1 and $f = (1 - \exp(-y^+/25)^3)^{0.5}$ for NT6. The computations were carried out on a Hitachi S-3800 machine and required up to 2 hours per cycle for NT1 to NT6 and 9 hours per cycle for NT7.

The group from the IIS (Kogaki *et al.* (1997), following in this volume) performed three simulations with varying resolutions, numerical methods and subgrid-scale models. Their first two simulations, IS1 and IS2, differed only in the spanwise resolution (though IS1 was sampled every ten time steps and IS2 every step for statistics). Both simulations used a Smagorinsky model with $C_s = 0.13$ and standard Van Driest damping functions close to the walls. The differencing schemes were second order (QUICK for the convection terms with Adams-Bashforth time advancement, central for other derivatives with Crank-Nicolson advancement). The inflow was standard and the outflow boundary condition convective. The simulations

were conditioned for 13 cycles before being sampled over a similar period. The cpu requirements were about 1.5 and 3 hours per shedding cycle on a Hitachi S-3800/480. The run IS3 was at higher resolution and required over 6 hours per shedding cycle on the same machine; as a result only half as many cycles were spent on both conditioning and sampling. The fifth-order upwind scheme was used for the convection terms and fourth-order central differences for diffusion terms. The same time-integration schemes were retained as in IS1 and IS2, but the run differed in utilising the dynamic mixed model of Vreman *et al.* (1994) and Zang *et al.* (1993), with the least-squares approach, stabilised by span averaging and bounding the viscosity below by the limit of zero viscosity.

The Science University group (Kawashima and Kawamura (1997), following in this volume) performed a set of four simulations, applying to this problem their convective schemes which act partially as subgrid models. The simulations differ slightly in the domain, meshing and sampling regimes. In several cases the convection schemes were used in combination with a Smagorinsky model. ST1 used central differencing and on the mesh employed was numerically unstable. In ST2 the UTOPIA convective scheme, which is a combination of fourth-order central and third-order upwind interpolation, was combined with the Smagorinsky model. ST3 omitted the Smagorinsky model entirely and relied on UTOPIA as a numerical model. ST4, with different lateral meshing, restricted the use of UTOPIA to the region $-3.5 < y/d < 3.5$; and ST5 utilised a different combination of fourth-order central and third-order interpolation in which the coefficient of the third order term, α, depends on the ratio of the Smagorinsky and molecular viscosities, thus: $\alpha = \exp(-\nu_t/100\nu)$; this we call the variable-alpha scheme. Otherwise the simulations use standard methods and boundary conditions, though the outflow was governed by zero streamwise gradient rather than the recommended convective condition, and the streamwise domain lengths varied; ST2 was performed in a rather short domain.

The group of the Tokyo Institute of Technology performed a single LES of some interest using embedded meshes. The outermost mesh was $121 \times 114 \times 27$, the middle mesh $113 \times 97 \times 57$ and the inner mesh which surrounded the cylinder was $91 \times 91 \times 127$. Diagrams of the meshing are given subsequently in this volume (Nozawa and Tamura, 1997). By this means the resolution close to the upstream face of the cylinder was made very fine (0.005) though somewhat coarser near-wall resolution was used on the cylinder sides (0.02) and rear faces (0.033). A third-order upwind scheme for the convection terms was combined with second-order differencing for the other terms and a subgrid eddy viscosity generated by a dynamic procedure applied to the Smagorinsky model with the least squares approach. The computation required 20 hours per cycle on one processor of a Fujitsu

VX.

The groups were invited to estimate the magnitude of the numerical dispersion and dissipation of their codes, but little data was submitted on this aspect of the LES apart from the specific studies of interaction between subgrid models and convection treatments by the IIS and SUT groups. Some of the submissions constituted a demonstration of the mesh dependence of the results; it does not appear that anyone was able to demonstrate mesh independence convincingly.

3. Results

The principal integral parameters predicted by the simulations in the exercise are shown in Table 3. The columns give the dataset followed by the predicted recirculation length, Strouhal number of the shedding, the drag and lift cofficients of the cylinder (the latter should be zero by symmetry) and the r.m.s. variation of the lift and drag.

TABLE 3. Results: Integral Parameters

set	l_r	St	C_D	C_L	r.m.s. C_D	r.m.s. C_L
UK1	1.32	0.13	2.20	-0.02	0.14	1.01
UK2	1.46	0.13	2.30	-0.04	0.14	1.15
UK3	1.44	0.13	2.23	-0.05	0.13	1.02
GRO	1.61	0.133	2.09	0.005	0.18	1.45
NT7	1.39	0.131	2.05	-0.05	0.12	1.39
UOI	1.20	0.13	2.03[b]	0.04	0.18	1.29
IS1	1.12	0.13	2.041	-0.29[e]	0.26	1.31
IS2	1.20	0.13	2.067	-0.0066	0.15	1.235
IS3	1.36	0.133	2.79	-0.125	0.36	1.68
TIT	1.23	0.131	2.62	0.0093	0.23	1.39
ST2	1.06	0.16	2.72	0.01	0.28	1.26
ST3	1.24	0.15	2.66	-0.005	0.27	1.33
ST4	1.12	0.139	2.74	0.012	0.29	1.36
ST5	1.02	0.161	2.78	0.009	0.28	1.38
LYN	1.38	0.132	2.1			
DUR	1.33	0.138				
LEE			2.05		0.16–0.23	
VIC			2.05			0.68–1.32
CLC			1.9–2.1		0.1–0.2	0.1–0.6
MAG			1.9–2.1		0.1–0.2	0.7–1.4

In the table the annotation ^{b} indicates that the drag coefficient has been corrected to allow for blockage, while ^{e} indicates a result which is affected by a known error, for instance in the boundary conditions. Some experimental results are given below the LES results: Lyn *et al.* (1995) (LYN) and Durao *et al.* (1988) (DUR) give the recirculation length and Strouhal number. Lee (1975) (LEE) gives a mean drag coefficient that agrees with a value given by Vickery (1966) (VIC), within the range found by Cheng *et al.* (1992) (CLC) and of McLean and Gartshore (1992) (MAG). These experiments were conducted under various conditions of free-stream turbulence and Reynolds numbers, but serve to indicate the general level of these quantities. There is broad agreement on the r.m.s. fluctuation of C_D, while the r.m.s. fluctuation of C_L is less clear from the experiments; it is probably in the region of 1.3.

It is not possible to show detailed output from all twenty datasets; we therefore select a subset for more detailed study. As the baseline solution (and to provide a bridge with the Rottach-Egern workshop) results from UK1 are included, and also those from UK3 which represents a significant advance in resolution. The results from Groningen (GRO) are based on a short sampling time and second-order moments have not converged sufficently to allow their inclusion; some results for the mean streamwise velocity only will be compared. Results are given for the finest resolution simulation of the Niigata-Tokyo group (NT7), for the simulation of the University of Illinois (IOU), and for the finest resolution simulation from the Institute of Industrial Science (IS3). The Tokyo Institute of Technology results, obtained on nested meshes, are included. Of the datasets submitted by the Science University of Tokyo group, the pure UTOPIA scheme appears to perform marginally better than the mixed scheme, Smagorinsky model, or the variable-alpha scheme, but is identical to a computation considered in the Rottach-Egern workshop; we therefore concentrate on the results from the variable-alpha scheme, ST5.

Thus in addition to UK1, we will present detailed results on one simulation from each group: UK3, GRO, NT7, UOI, IS3, TIT and ST3. These datasets are highlighted in bold in Table 3.

Many of the LES have difficulty in estimating the recirculation length. As we shall see, even quite credible streamwise profiles of U may still cross the $U = 0$ axis at the wrong position. Given the difficulty of getting l_r right, the performance of simulation NT7 seems impressive: this simulation predicts most of these integral parameters correctly, apart from the r.m.s. lift which may be low. However, we shall see that in other respects this simulation may be at fault. The group give some mean integral quantities as a diagnostic for their test runs NT1 to NT6; these results are summarised in Table 4. The lift coefficients, also estimated, were acceptably low. Several

runs appear to be heading towards good mean values on the basis of these criteria, including NT6.

TABLE 4. Recirculation lengths and drag coefficients for runs NT1 to NT6

run:	NT1	NT2	NT3	NT4	NT5	NT6
l_r	1.11	1.37	1.28	1.45	1.43	1.31
C_D	2.10	2.08	2.06	2.12	2.09	2.03

The Strouhal number was found to be relatively easy to predict correctly both in this exercise and at Rottach-Egern. The rather high values found by the Science University group in runs ST2 and ST5 (also ST3 to some extent) are worrying, possibly indicating a deleterious effect of resolution or the special numerical schemes, including the variable-alpha scheme.

4. Discussion

Figure 2 shows the streamwise distributions of normalised mean streamwise velocity and turbulence intensities over selected ranges of x downstream of the cylinder along the centreline. It is immediately apparent that the problem of predicting the recovery of the centreline velocity (2a, top), noted at Rottach-Egern, has not been solved conclusively. The experiment shows the velocity reaching about 0.6 of the upstream free-stream level and then apparently tending to level off (though data were not taken beyond $x/d = 8$). Some of the LES, in particular UK1, UK3 and NT7, show the velocity approaching the original level; others such as TIT and UOI show a distinct decline beyond about $x/d = 5$, which is difficult to understand physically although it is not necessarily incompatible with the experimental data shown, which appears to be levelling off at $x/d = 8$.

Figure 2b (top) is a view of U in the recirculation zone and up to $x/d = 3$. We note that those simulations having the lowest velocity at their exit planes are those with the shortest recirculation lengths (TIT and UOI) while some simulations that recover towards $U/U_0 = 1$, such as NT7 and UK3, have longer recirculation lengths. The simulation GRO, without a subgrid model, has a long recirculation length but a reasonable recovery further downstream — a result that is confirmed by the comparisons made by Wang and Vanka (1996) with and without a subgrid model, though in their case the rather short recirculation was actually improved by removing the model.

It would appear that the simultaneous prediction of the recirculation bubble length and the final recovery of the centreline velocity is still diffi-

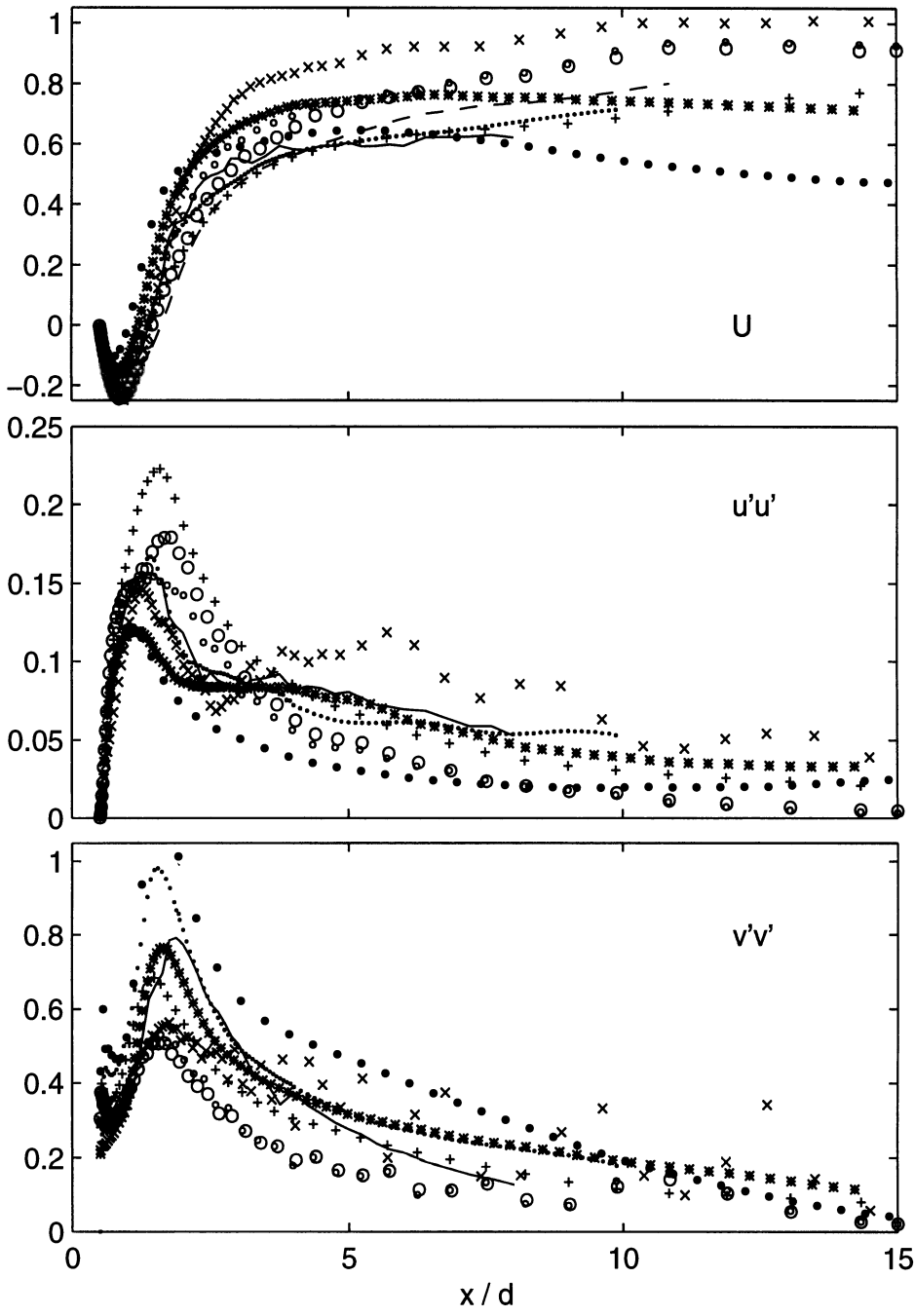

Figure 2. (a) Streamwise distributions of mean U and stresses along the centreline $y = 0$ for $x < 15$; Solid line, experiment of Lyn *et al.*; symbols, simulations: GRO dashed line (U only); UK1 ∘ ; UK3 ◯ ; UOI ∗ ; NT7 × ; IS3 + ; TIT • ; ST5 ● .

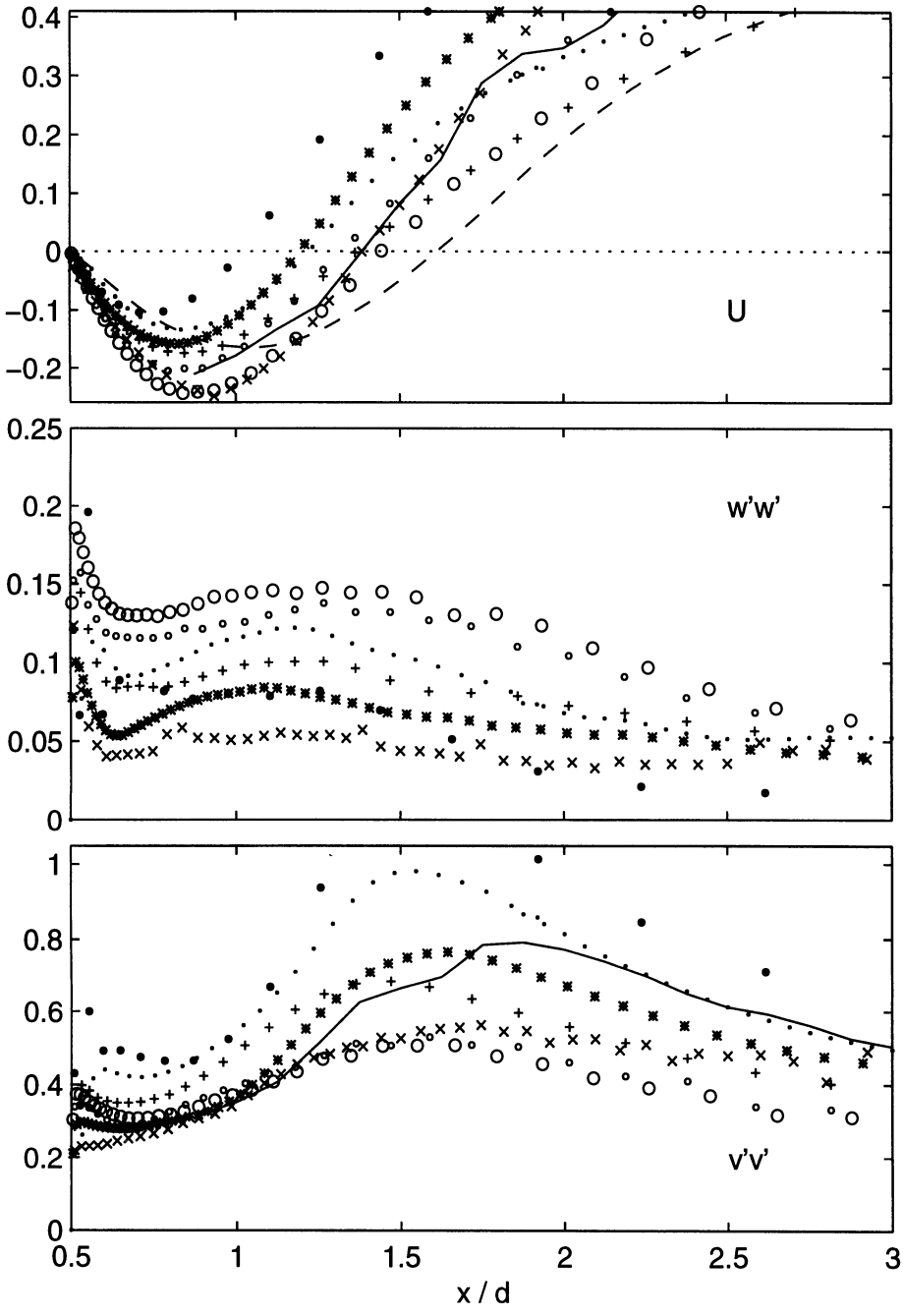

Figure 2. (b) Streamwise distributions of mean U and stresses along the centreline $y = 0$ for $x < 3$. As Fig. 2a

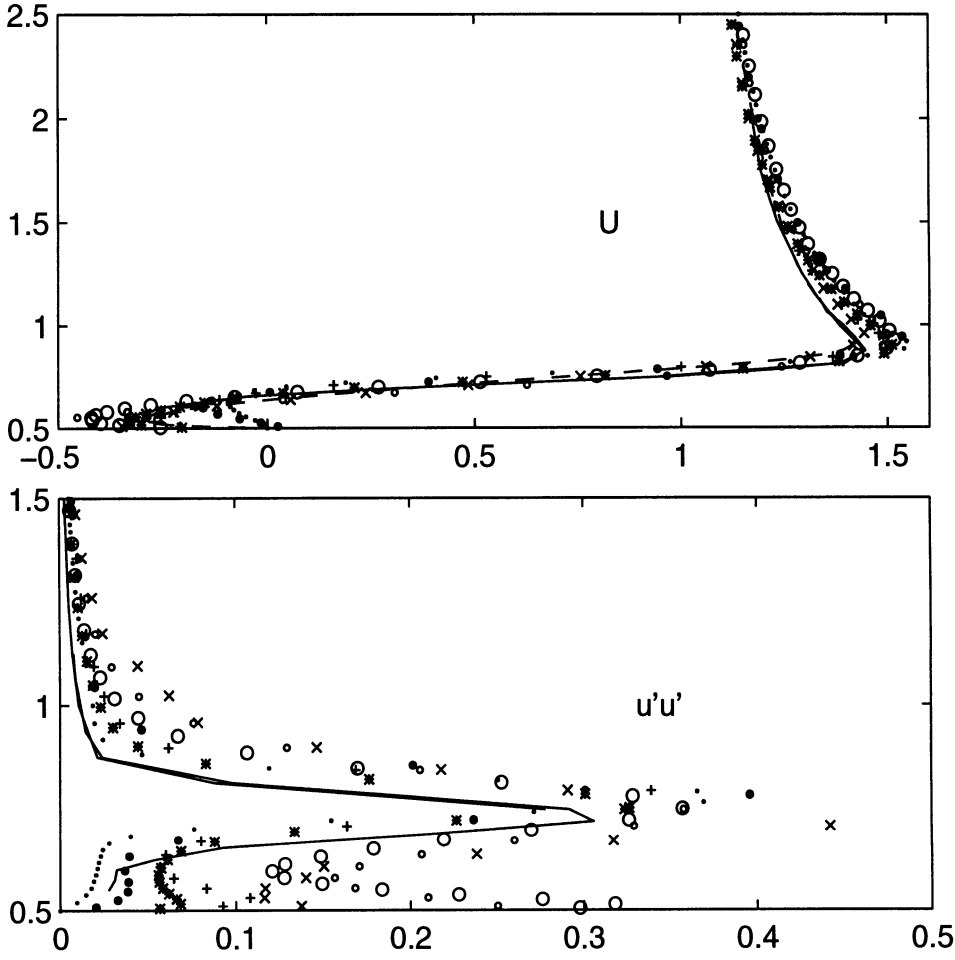

Figure 3. (a) Profiles of mean U and stress u'^2 at $x = 0$, the cylinder centre. Solid line, experiment of Lyn *et al.*; symbols, simulations, as Figure 2. The vertical co-ordinate is y.

cult. The diffusion of streamwise momentum towards the centre is affected by the subgrid terms and presumably also by numerical effects which are not yet fully elucidated. It is possible that the stretching of the x mesh and the resolution further downstream, which differ between the groups, is a major factor influencing the numerical diffusion, as suggested by Pourquié *et al.* (following paper).

Of the submissions shown here, IS3 has both a convincing centreline recovery and recirculation length; however a close inspection suggests there may be some good fortune in the latter prediction, and the high drag coefficient of this run is not reassuring. It is certainly premature to recommend

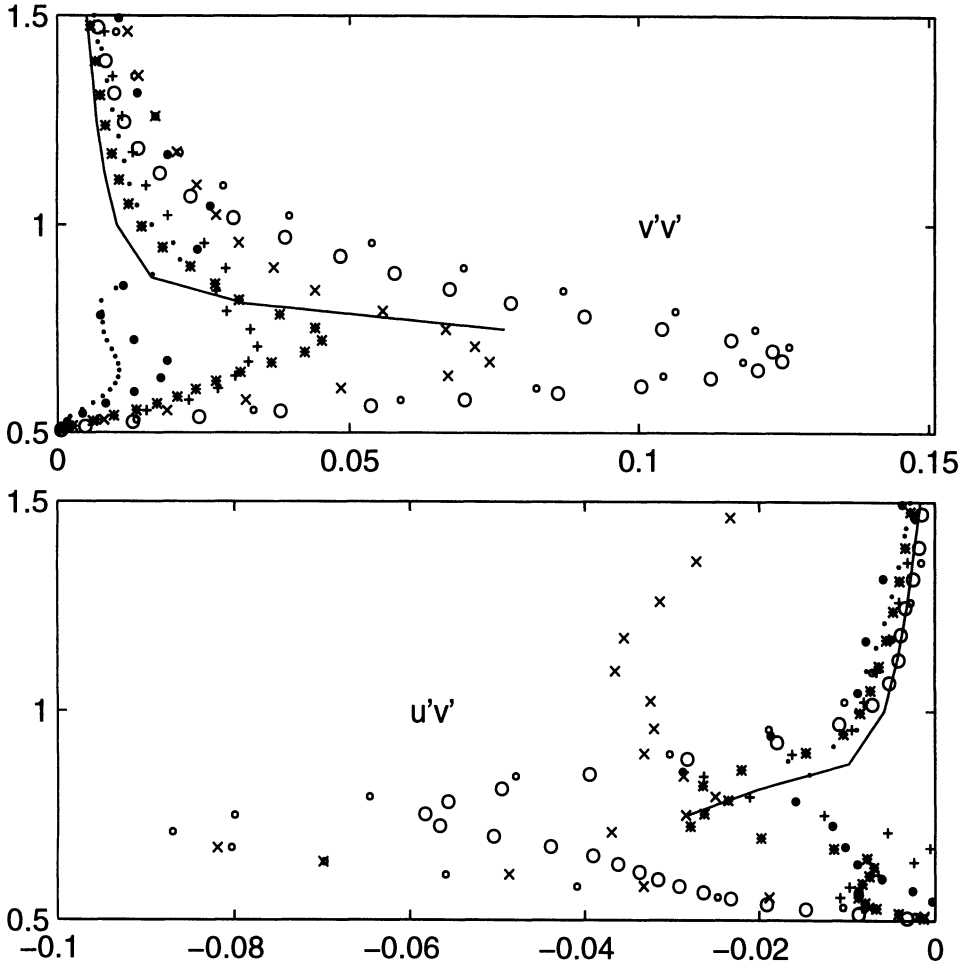

Figure 3. (b) Profiles of turbulence stresses at $x = 0$, the cylinder centre, as labelled. As Figure 3a.

a particular method from these results.

The predictions of stresses along the centreline also shown in Figure 2 confirm the view that no simulation is perfect. These are the full stresses comprising turbulent and coherent motions. NT7 suffers from some statistical scatter, and other simulations, while better converged statistically, fail to reveal systematic advantages or defects. There is no experimental data for w'^2, nor predictions of stresses from GRO. The expanded views of v'^2, Fig. 2b, reveal a tendency for all the LES to place the peak slightly closer to the rear face of the cylinder (at $x/d = 0.5$) than the experiment. The fact that all the simulations fail to resolve the inner peaks in v' and, especially,

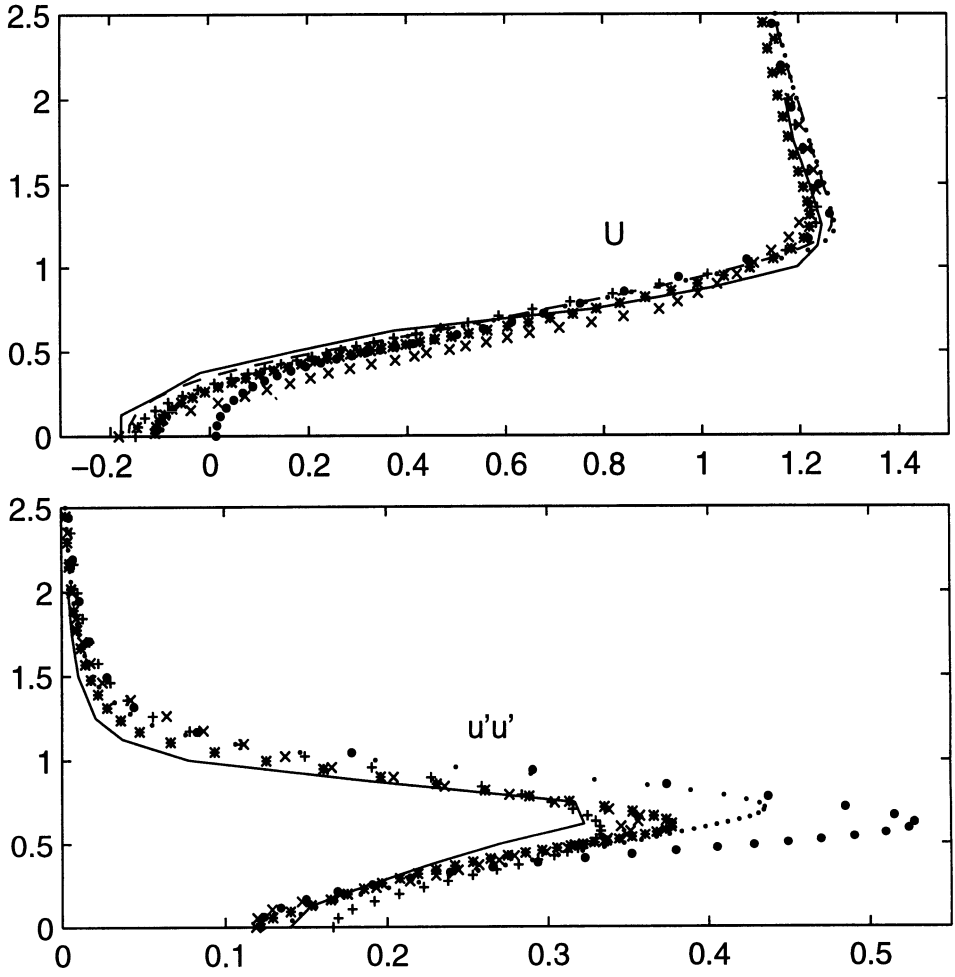

Figure 4. (a) Profiles of mean U and stress u'^2 at $x = 1$, in the recirculation, as labelled. Solid line, experiment of Lyn *et al.*; symbols, simulations, as Figure 2. The vertical co-ordinate is y.

w' also shows that we have inadequate resolution on the back face of the cylinder.

Figure 3 shows profiles in the centre of the top surface of the cylinder. Agreement for U is adequate, but for the components of the stress the variable behaviour of the different numerical schemes and models is abundantly clear. Some methods predict a large spike of u'^2 very close to the wall, presumably the result of reverse shear at the wall inside the recirculation bubble, in contrast to the experiment. Again no one simulation shows a clear advantage in all the quantities plotted.

Figure 4, giving profiles at $x = 1$ which cuts the mean recirculation,

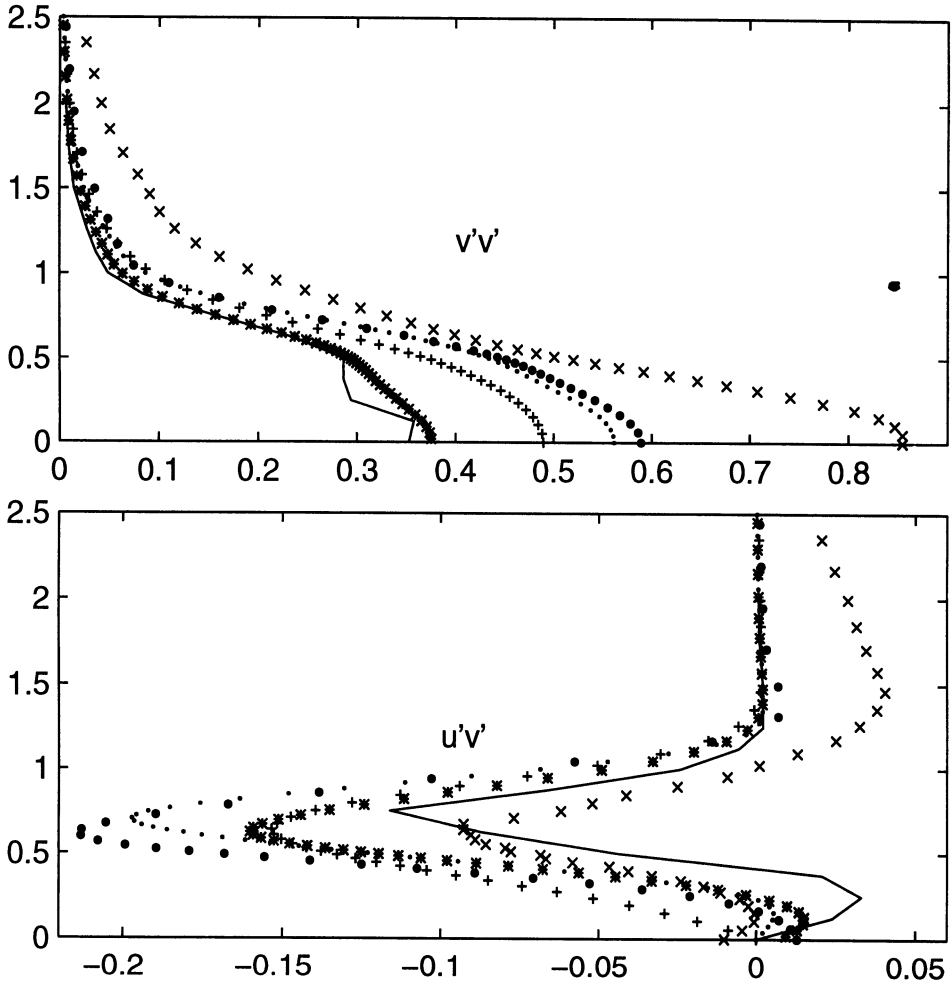

Figure 4. (b) Profiles of mean stresses at $x = 1$, as labelled.

reveals that at this point there is some agreement on the shape of the mean velocity profile, but already great variation in the predicted vertical fluctuation and the principal shear stress. Clearly, with such a variation in the magnitude (and also extent) of vertical mixing, the simulations will inevitably have widely divergent rates of filling of the wake. At this station, the results of the UOI simulation are qualitatively and quantitatively the closest to the experiment.

By the $x = 5$ station, the effects of the different rates of filling of the wake are readily apparent in the mean velocity profiles, Figure 5. Since even the mean shear rates are quite different between the simulations, we are not surprised to find qualitatively divergent pictures from the various groups.

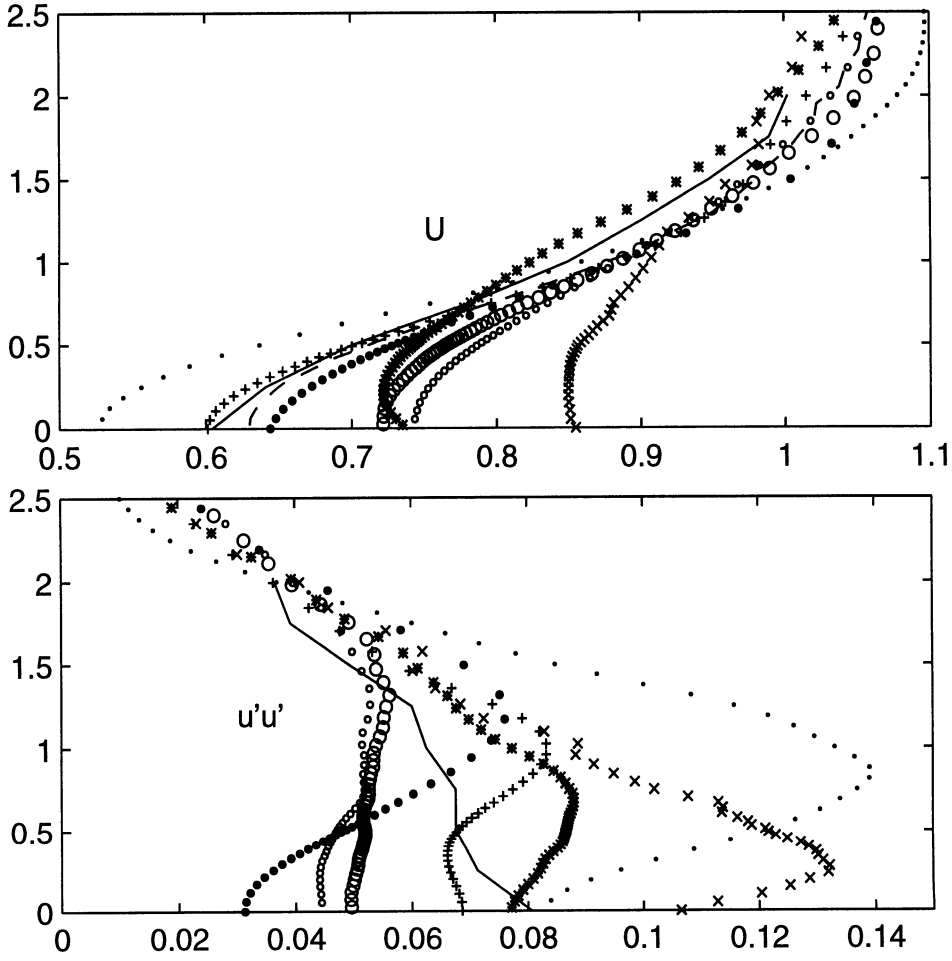

Figure 5. (a) Profiles of mean U and stress u'^2 at $x = 5$, beyond the recirculation. Solid line, experiment of Lyn *et al.*; symbols, simulations, as Figure 2. The vertical co-ordinate is y.

Most of the simulations seem to suggest a central dip in u' at this stage, unfortunately not supported by the experimental data used for comparison. The vertical fluctuations are still widely disparate, though the picture for v' is not simply a reflection of the situation obtaining at $x = 1$; NT7, which overpredicts the v' fluctuations at $x = 1$ has dropped back by $x = 5$, and in fact has a worryingly low level of Reynolds stress in the central portion of the wake.

Contours of these quantities in the x–y plane were produced from submitted data and discussed at the workshop. The foregoing comments reflect insights gained from these two-dimensional distributions.

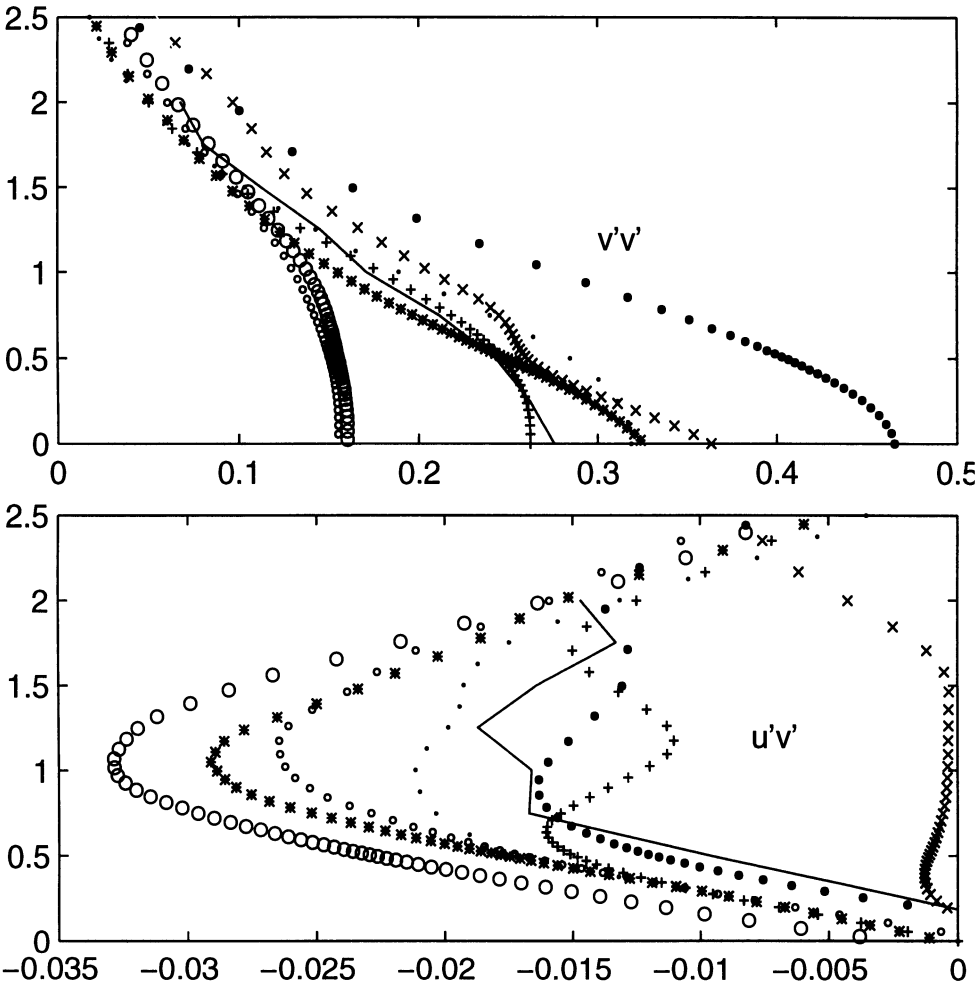

Figure 5. (b) Profiles of mean stresses at $x = 5$, as labelled.

5. Conclusions

In the light of the great variation in the predictions of the simulations around the cylinder, it is still not possible to make any recommendations apart from the obvious one that higher resolution is required at the walls. For the near wake region, IS3 and UOI, two simulations performed completely independently using higher order upwind schemes, dynamic models and somewhat similar meshing, produce reasonable quantitative predictions on many scores and an overall impression of qualitative agreement. We might be tempted to conclude that, at least for the wake region, this combination of methods has much to recommend it, though the data pro-

duced in this exercise are not extensive enough to indicate a clear advantage of particular methods or models at present.

These simulations, which give reasonable qualitative predictions in the wake while still having a number of clear faults, are among those using higher spanwise resolution. Only the rather special simulations GRO and TIT use higher spanwise resolution, and the latter only for its restricted, embedded meshes. In the light of the structural differences shown by Kogaki *et al.* (following paper) as the spanwise resolution is changed, it appears that the spanwise meshing used by many of the submissions is inadequate to deal with the breakdown of the flow to three dimensions behind the cylinder. It would be wise, in any future studies of this test case, to use a minimum of 32 meshes across the domain width of $4d$.

The other main conclusion is less firm, being based on the wide variation of predictions of the vertical fluctuation, resolved Reynolds stress, and rate of filling of the wake. The latter disagreement is presumably simply a natural consequence of the former. While different subgrid models or discretisation schemes may be partly to blame for the wide divergence of the predictions, another possibility is the different rates of stretching of the x mesh in the region downstream of the cylinder. M. Pourquié pointed out at the workshop that his centreline filling can be brought into line with the experiment simply by retaining a fine x mesh (with low stretching); his remarks were based on a further simulation, UK4, not included in this study and to be completed. It is important to verify if this is indeed the case independently of other variations such as the model or numerical scheme employed. Discussion at the workshop mentioned that rapid stretching of the mesh in the streamwise dimension can have radical and as yet poorly understood effects on simulated turbulence, as resolved eddies are advected onto a mesh that can no longer resolve them.

The flow over and following the square cylinder is therefore proving a major challenge to current LES techniques, a stimulus to further investigation and a problem to which, at present, we cannot claim to have a definitive solution.

Acknowledgements

The author acknowledges his debt to the separate contributors to this exercise, who produced amd submitted a large amount of data in remarkable accord with the required formats. In particular, the contribution of Dr Pourquié is acknowledged in providing datasets UK1 and UK3, setting up the test case LES2 and co-operating in presenting the background of the exercise. Thanks also go to Professors Rodi and Ferziger for their initiative in first setting this test case.

References

CHENG C.M., LU P.C. & CHENG R.H. (1992) Wind loads on square cylinders in homogeneous turbulent flows, *J. Wind Eng. Ind. Aero.* **41**, 729.

DURAO D.F.G., HEITOR M.V. & PEREIRA J.C.F. (1988) Measurements of turbulent and periodic flows around a square cross-section cylinder. *Exp. Fluids* **6**, 298.

KAWASHIMA N. & KAWAMURA H. (1997) Numerical analysis of LES of flow past a long square cylinder. Following in this volume.

KOGAKI T., KOBAYASHI T. & N. TANIGUCHI (1997) LES of flow around a square cylinder. Following in this volume.

LEE B.E. (1975) The effect of turbulence on the surface pressure field of a square prism, *J. Fluid Mech.* **69**, 263.

LYN D.A. & RODI W. (1994) The flapping shear layer formed by flow separation from the forward corner of a square cylinder, *J. Fluid Mech.* **267**, 353.

LYN D.A., EINAV S., RODI W. & PARK J.H. (1995) A laser-Doppler velocimetry study of ensemble averaged characteristics of the turbulent near wake of a square cylinder, *J. Fluid Mech* **304**, 285.

MCLEAN I. & GARTSHORE I. (1992) Spanwise correlations of pressure on a rigid square cylinder, *J. Wind Eng. Ind. Aero.* **41** 797.

MURAKAMI S., MOCHIDA A., TOMINAGA Y.& IIZUKA S. (1997) LES analysis of turbulent flow past a square cylinder using various SGS models. Following in this volume.

NOZAWA K. & TAMURA T. (1997) LES of flow past a square cylinder using embedded meshes. Following in this volume.

RODI W., FERZIGER J.H., BREUER M. & POURQUIÉ M. (1996) Status of Large Eddy Simulation: Results of a Workshop. *J. Fluids Eng.* To appear.

VERSTAPPEN R.W.C.P. & VELDMAN A.E.P. (1997) Fourth-order DNS of flow past a square cylinder: first results. Following in this volume.

VICKERY B.J. (1966) Fluctuating lift and drag on a long square cylinder of square cross-section in a smooth and in a turbulent stream, *J. Fluid Mech.* **25**, 481.

VREMAN B., GEURTS B. & KUERTEN H. (1994) On the formulation of the dynamic mixed subgrid scale model. *Phys. Fluids* **6** (12) 4057.

WANG G. & VANKA S.P. (1996) Large Eddy Simulations of High Reynolds Number Turbulent Flow Over a Square Cylinder. *Report CFD 96–02*, Computational Fluid Dynamics Laboratory, Dept. Mech & Ind. Engineering, University of Illinois at Urbana–Champaign, IL 61801.

WANG G. & VANKA S.P. (1997) LES of flow over a square cylinder. Following in this volume.

WERNER H. & WENGLE H. (1993) Large-eddy simulation of turbulent flow over and around a cube in a plane channel, *Turbulent Shear Flows 8* (ed. Durst *et al.*) Springer-Verlag, Berlin. pp 155–168.

ZANG Y., STREET R.L. & KOSEFF J.R. (1993) A dynamic mixed subgrid-scale model and its application to turbulent recirculating flows, *Phys. Fluids* **A5** (12) 3186.

COMPUTED TEST CASE: SQUARE CYLINDER

M. POURQUIE, M. BREUER AND W. RODI
Institute for Hydromechanics,
University of Karlsruhe, Germany

1. Overview

Three calculations made with the LESOCC code have been completed. LESOCC is a second order accurate finite volume method on a collocated grid in general curvilinear coordinates, used for the calculations at the Rottach–Egern workshop. Two were presented at the Rottach-Egern workshop (UKAHY1 and UKAHY2, called UK1 and UK2 here). It was decided to continue runs with the UK2 grid, since in the case of the UK1 grid the near wall boundary resolution was very probably inadequate. The main aim is to check some of the conclusions, reached at the Rottach-Egern workshop. Among others, conclusions were made regarding the use of wall laws. UK3 is new; it is equivalent to UK2 except that no wall function was used but a simple no-slip BC. It allows conclusions regarding the use of a wall law.

Results for UK2 and UK3 (wall law versus no-slip) look qualitatively the same. Our conclusion so far is that the effect of the wall law on at least some of the bulk parameters is indeed small. Two examples are discussed, namely recirculation length and drag coefficient (see the table in the next section). One conclusion made at the Rottach–Egern workshop, namely that the recirculation length is shorter for simulations using no wall function, is not in agreement with what is found here: the recirculation lengths for UK2 and UK3 are only marginally different. A possibility is that one finds a shorter recirculation region when no wall law is used and one has at the same time a coarse grid near the cylinder, which was the case for the calculations presented at the Rottach–Egern workshop. Since the drag coefficient is related to the recirculation length (a shorter recirculation length corresponding with a higher drag coefficient and vice versa) an analogous conclusion for the drag coefficient, namely that using no wall law means obtaining a higher drag, also does not hold provided enough resolution is used.

J.-P. Chollet et al. (eds.), Direct and Large-Eddy Simulation II, 375-379.

All of the runs made so far show the same, quick recovery of the mean velocity component in the main stream direction. This is connected with the resolution far away from the cylinder.

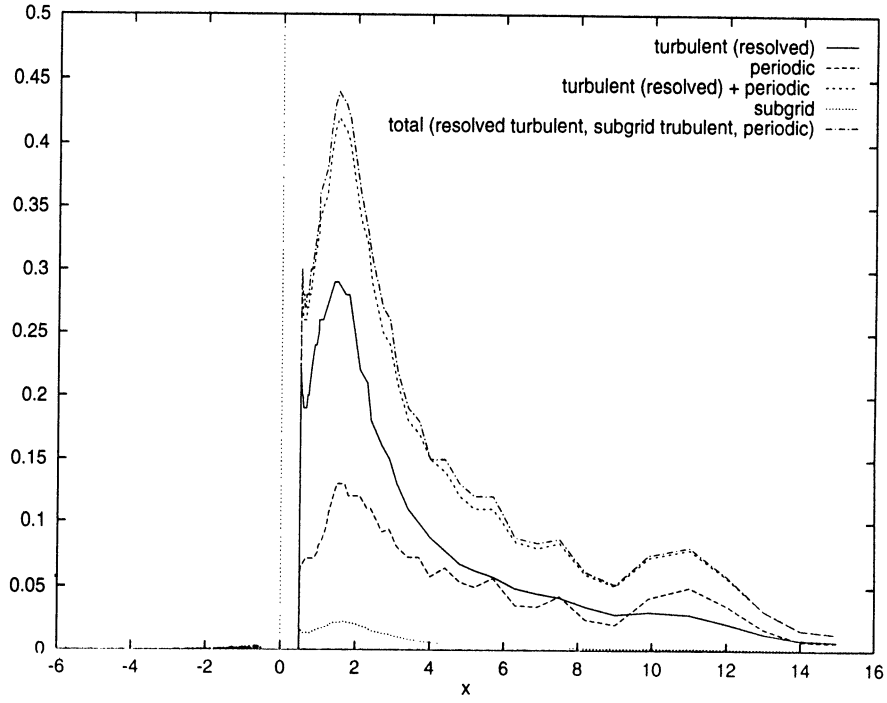

Figure 1. Values for the fluctuations (total, turbulent, periodic, subgrid) on the centerline: UK3

The influence of the SG terms is more fully investigated. Using Mason's (1983) estimate for the subgrid energy, we get the following picture, Figure 1, for the relative order of magnitude of SGE and resolved energy on the centerline. We distinguish between resolved (total), periodic, turbulent and subgrid component. One question here is what to compare the SG part with: with the total fluctuation or only with the turbulent. For this reason the turbulent part was included in the figure, although the phase averaging method used to obtain the turbulent part separately has some points which need further discussion. Moreover, other estimates than Mason's may give higher values for the SG part. However, we can assess whether the SGE is small compared to the resolved energy (on the centerline). Of course, for an LES one wants the SG energy to be much smaller than the resolved energy. If we use the criterion that the SG part of the turbulent kinetic energy should be less than 10% of the total fluctuation or even only the turbulent part, then we meet this criterion (on the centerline) if we use Mason's estimate.

Summarizing, some conclusions of the Tegernsee Workshop have been considered using calculations UK2 and UK3 using respectively Smagorinsky wall–law and Smagorinsky no–slip. Moreover, the SG energy content on the centerline has been found to be small enough compared to the resolved motion to meet the 10% criterion if we use Mason's estimate and compare SG energy with only the turbulent part of the resolved energy.

2. Details of calculations

2.1. GEOMETRY OF COMPUTATIONAL DOMAIN AND GRID

The calculation domain, viewed from the center of the cylinder is given by: $4D$ in periodic direction, $5D$ in front of the origin (= $4.5D$ in front of cylinder), $15D$ after the origin (= $14.5D$ after the back of the cylinder). The grids are equidistant in the direction of the cylinder axis. In the other two directions they are non–equidistant, generated with the aid of geometric series, separately for the region in front of the cylinder, above and below the cylinder, and behind the cylinder. A maximum distance from the wall is given for the grid cells nearest to the cylinder wall, and the stretching factor is not allowed to become larger than 1.1. As a result, the following three grids are applied:

Key	Total no. of grid points	grid points left–right	grid points bottom–top	along axis	grid size near wall
UK1	$109 \times 105 \times 20$	33, 29, 45	37, 29, 37	20	0.02
UK2	$146 \times 146 \times 20$	52, 40, 52	52, 40, 52	20	0.01
UK3	$146 \times 146 \times 20$	52, 40, 52	52, 40, 52	20	0.01

Resolution on the cylinder:

Key	Grid points on cylinder
UK1	29×29
UK2	40×40
UK3	40×40

Stretching factors are always smaller than 1.1.

BOUNDARY CONDITIONS

At the inflow plane constant velocity is imposed (no perturbations added). A convective boundary condition is utilized at the outflow boundary.

Werner & Wengle's wall function approach (1993) is applied on the cylinder walls for UK1 and UK2; for UK3 we used a simple no-slip BC. At the lateral walls free–slip conditions are used. Periodic boundary conditions are applied in the spanwise direction of the cylinder.

2.2. NUMERICAL METHOD

The code developed at the Institute for Hydromechanics, University of Karlsruhe, Germany, is based on a finite–volume method for solving the incompressible Navier–Stokes equations on general body–fitted, curvilinear grids (LESOCC = **L**arge **E**ddy **S**imulation **O**n **C**urvilinear **C**oordinates). A non–staggered, cell–centered grid arrangement is used. Both convective and viscous fluxes are approximated by central differences of second order accuracy. The temporal discretization consists of a predictor–corrector scheme, where the predictor step is an explicit Adams–Bashforth scheme for the momentum equations (second order in time) and the corrector step covers the implicit solution of the Poisson equation for the pressure correction (SIMPLE). The linear system is solved by the strongly implicit procedure of Stone which is accelerated by a FAS multigrid technique. In order to avoid decoupling of pressure and velocity on the non–staggered grid the momentum interpolation proposed by Rhie and Chow (1983) is applied.

2.3. SUBGRID–SCALE MODELS

Two different subgrid–scale models are implemented, the standard Smagorinsky model with Van Driest damping ($l = C_s\Delta(1 - \exp(-y^+/25)^3)^{0.5}$) and the dynamic model. In the calculations reported here, only the Smagorinsky model is used.

2.4. COMPUTER RESOURCES

All computations are performed on the mainframe Fujitsu VP S600/20 installed at the Computer Center of the University of Karlsruhe. It has a peak performance of 5 Gflops and a core memory of 2 Gbytes. The code written for curvilinear body–fitted coordinates is much more general applicable than for the test cases of the workshop which can be done by applying simple Cartesian grids. It should be noted that *no* tuning is done for the specific test cases which results in higher computing costs compared to a

program written especially for Cartesian coordinates and applying special algorithms.

Key	time step Δt	time for sampling	simulation time	time steps	CPU time (hours)
UK1	10^{-3}	$104t*$	200 t*	104000	≈ 33
UK2	4×10^{-4}	$64t*$	128 t*	160000	≈ 72
UK3	4×10^{-4}	$96t*$	140 t*	175000	≈ 80

Sampling rate was every t*/20.

2.5. BULK QUANTITIES

calculation	rec len.	St	Cd	Cl	rms Cd	rms Cl.
UK1	1.32	.13	2.20	-0.02	.14	1.01
UK2	1.46	.13	2.30	-0.04	.14	1.15
UK3	1.44	.13	2.23	-0.05	.13	1.02

TABLE 1. Some bulk quantities for three cylinder calculations

References

Rhie, C.M., Chow, W.L.: *A numerical study of the turbulent flow past an isolated airfoil with trailing edge separation,* AIAA-J., Vol. 21, pp. 1225–1532, (1983).

Werner, H., Wengle, H.: *Large-Eddy Simulation of Turbulent Flow Over and Around a Cube in a Plane Channel,* Turbulent Shear Flows 8, (ed. Durst *et al.*), Springer-Verlag, (1993).

FOURTH-ORDER DNS OF FLOW PAST A SQUARE CYLINDER: FIRST RESULTS

R.W.C.P. VERSTAPPEN AND A.E.P. VELDMAN
Department of Mathematics, University of Groningen, P.O.Box 800, 9700 AV Groningen, The Netherlands

Abstract. In this paper we present some initial results of a fourth-order direct numerical simulation of flow past a square cylinder at $Re = 22,000$. The flow is identical to the second test case which is considered at this workshop. Mean velocities, the mean Strouhal number, the mean drag coefficient Cd, the mean lift coefficient Cl and the rms fluctuations of Cd and Cl are computed.

1. Introduction

In another paper in this volume (Verstappen and Veldman, 1996), we present a comparison between two DNS methods: a well-known second-order finite volume method and a fourth-order finite volume method which is constructed as the Richardson extrapolate of the second-order method. These two approaches are compared for a turbulent flow in a cubical lid-driven cavity at Re = 10,000. Experimental results are available for comparison. The fourth-order method turns out to be the best (see e.g. Figure 3 of that paper).

In this paper we consider a test case of this workshop, the flow past a square cylinder at $Re = 22,000$ at zero angle of attack. Also for this test case we find the fourth-order method performs better than the second-order method. On a $280 \times 210 \times 64$ grid all our second-order simulations failed due to insufficient spatial resolution, while the fourth-order simulation method performed well.

However, even using a fourth-order DNS method the flow past a square cylinder at $Re = 22,000$ is an expensive nut to crack: one shedding cycle takes about 40 hours on 16 nodes of a Cray J932. Up till now, the fourth-order DNS has taken several hundreds of CPU-hours. The simulation has

J.-P. Chollet et al. (eds.), Direct and Large-Eddy Simulation II, 381-384.

not finished completely: the start-up of the flow plus three shedding cycles have been computed, and limited results based on this part of the simulation are presented.

Unfortunately we cannot compute sensible average values of turbulence intensities or Reynolds stresses from the three shedding cycles that are available now: a period of three shedding cycles is simply too short. However, some first results — mean velocities, the mean Strouhal number, the mean drag coefficient Cd, the mean lift coefficient Cl and the root-mean-square fluctuations of Cd and of Cl — can be computed. These results are presented in Section 3. Before that, some details of the simulation are given.

2. Details of the simulation

We use for this test case the prescribed coordinate system, which has its origin at the centre of the cylinder, and normalise all quantities by the cylinder width and the inflow velocity. The streamwise direction is denoted by x, the lateral direction by y and the spanwise (periodic) direction by z. The components of the velocity in these directions are u, v and w, respectively.

The inflow boundary is located at $x = -7$, i.e., six and a half diameters upstream of the cylinder. The inflow condition is $u = 1$, $v = 0$, $w = 0$. The lateral boundaries are located at $y = \pm 7$. At these boundaries we have imposed $u_{yy} = w_{yy} = p_y = 0$, where p is the pressure. The outflow boundary is located at $x = 20$. The outflow conditions are $v_{xx} = w_{xx} = 0$ and $p_x =$ constant, where the constant is determined such that the mass inflow equals the mass outflow at each time-step; this constant is approximately zero. In addition, in a buffer zone ($x = 15.0-20.0$) the Reynolds number is decreased from 22,000 to 1,000 to suppress (unphysical) waves which are reflected by the artificial outflow boundary. The spanwise boundaries are four diameters apart. No-slip boundaries are imposed at the cylinder surface.

We have used a $280 \times 210 \times 64$ (stretched and staggered) grid to cover the computational domain. The first meshpoint is spaced $5 \times 10^{-3} d$ from the cylinder surface. The grid is stretched away from the cylinder surface using a sinh function; the ratio of the largest to smallest gridsize is approximately 200 (in x) and 100 (in y). The time-step equals 10^{-3}, and statistics are sampled at each time-step.

The numerical method is identical to the one that is described in Verstappen and Veldman (1996). It should be emphasized that in that paper, and also here, we have used constant weights (9/8 and -1/8) in the Richardson extrapolation. The reason for this is that the higher-order discretization thus obtained is conservative. If the weights are adapted to the stretching of the grid to obtain a formally more accurate scheme, the result is non-conservative.

The convective flux is integrated in time using a modified second-order Adams-Bashforth method. According to Adams-Bashforth we ought to take $\frac{3}{2}f(u^n) - \frac{1}{2}f(u^{n-1})$; instead we take $f(\frac{3}{2}u^n - \frac{1}{2}u^{n-1})$. The two approaches differ when the right-hand side f is non-linear. For instance for $f(u) = \lambda(t)u$ with $\lambda(t) < 0$ and $u^n > 0$ the numerical solution u^{n+1} of $u_t = f(u)$ is smaller than u^n (for any time step) as it should be, while the solution obtained with the original Adams-Bashforth method does not satisfy the inequality $u^{n+1} < u^n$ unconditionally.

The discrete Poisson equation for the pressure is solved using a combination of a fast Fourier transform method in the spanwise direction and a modified incomplete Choleski conjugate gradient method in the resulting spectral space. After the Fourier transform (which can be computed in parallel over the x and y directions), the discrete Poisson equation falls apart into a set of mutually independent 2D equations with additions to their diagonals due to the Fourier transform. This set of mutually independent equations is distributed over the processors and solved. Thus a 100% parallel implementation is achieved.

3. Predicted data

In this section averages are shown which are computed over three shedding cycles and the spanwise direction. Velocities are also averaged over the top and bottom halves. Table 1 shows the mean Strouhal number, the mean drag coefficient Cd, the mean lift coefficient Cl and the root-mean-square fluctuations of Cd and Cl. The experiment is described in Lyn et al. (1995).

TABLE 1. Comparison of DNS with experiment

	DNS	Experiment
Mean Strouhal number	0.133	0.130 - 0.137
Mean drag coefficient Cd	2.09	1.9 - 2.1
Mean lift coefficient Cl	0.005	-
Rms fluctuation of Cd	0.178	0.1 - 0.2
Rms fluctuation of Cl	1.45	0.6 - 1.4

It may be noted that the mean lift coefficient has not been measured; it should be zero. So far, we have only computed three full shedding cycles, yet the computed values of all bulk quantities falls within the range set by the experiment except for the root-mean-square of the fluctuations of the lift coefficient Cl. The rms fluctuation of Cl seems to be slightly overestimated by the DNS.

Figure 1 shows the mean streamwise velocity at four locations past the cylinder.

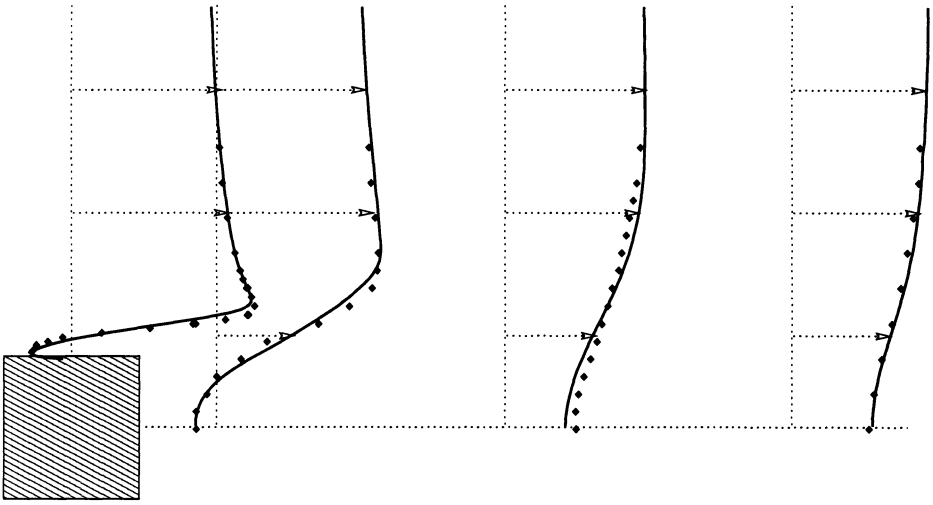

Figure 1. A comparison of mean velocities of the DNS with experimental results. The experimental data is taken from ERCOFTAC Database Case 43; see also Lyn *et al.* (1995). Shown is the mean streamwise velocity at x=0, x=1, x=3 and x=5. Continuous lines, DNS; dots, experimental data.

Acknowledgements

The Stichting Nationale Computerfaciliteiten (National Computing Facilities Foundation, NCF) with financial support from the Nederlandse Organisatie voor Wetenschappelijk Onderzoek (Netherlands Organization for Scientific Research, NWO) is gratefully acknowledged for the use of supercomputer facilities.

References

Verstappen, R.W.C.P. and Veldman, A.E.P. (1996), A comparison of low-order DNS, high-order DNS and LES. *Direct and Large-Eddy Simulation II*, (eds J.P. Chollet *et al.*) This Volume.

Lyn, D.A., Einav S., Rodi W. and Park J.H. (1995), A laser-Doppler velocimetry study of ensemble averaged characteristics of the turbulent near wake of a square cylinder, *Journal of Fluid Mechanics* **304**, 285.

LES ANALYSIS OF TURBULENT FLOW PAST A SQUARE CYLINDER USING VARIOUS SGS MODELS

S. MURAKAMI AND S. IIZUKA
I.I.S., University of Tokyo,
7-22-1, Minato-ku, Roppongi, Tokyo, 106, Japan
AND
A. MOCHIDA AND Y. TOMINAGA
Niigata Institute of Technology,
1719, Fujihashi, Kashiwazaki, Niigata, 945-11, Japan

1. Outline of computations

The turbulent vortex shedding flow past a two-dimensional square cylinder at $Re=2.2x10^4$ (test case LES2) was analyzed by Large Eddy Simulation using various dynamic subgrid-scale (SGS) models [1-5]. The types of SGS model used are as follows: the static type of conventional Smagorinsky model (S model, eqns.(1) and (2) in the Appendix (case 1)); the Dynamic Smagorinsky model (DS model, eqn.(6) in the Appendix (case 2)); the Dynamic Mixed model (DM model, eqn.(10) in the Appendix (case 3)); and the Lagrangian Dynamic Mixed model (LDM model, eqn.(16) in the Appendix (case 4)).

Table 1 lists the 7 cases computed. Computations were carried out for three different computational grids (grids A-C), two different grid systems (colocated and staggered grids) and four different SGS models. Details of SGS models compared here are given in the Appendix. Preliminary computations were carried out on a relatively coarse grid (grid A) using four types of the SGS models in cases 1-4. The relative performance of these four SGS models was clarified by comparison with those given from the experiment by Lyn *et al.* [7]. As is described later, the LDM model (case 4) provided the best results.

A colocated grid was used in cases 1-4. In case 5, a computation using a staggered grid was carried out in order to assess the difference in prediction accuracy between the colocated grid and staggered grid. In case 6, we carried out the computation with the same conditions as those of the computation UKAHY1 by the University of Karlsruhe group for the 1995 Workshop of LES of Bluff Body Flows (Rottach-Egern workshop) [6]. The results of case 6 were compared with those of case 1. Finally, a computation using the LDM model was carried out with a grid spacing (grid C) which was finer than grid A used in

J.-P. Chollet et al. (eds.), Direct and Large-Eddy Simulation II, 385-395.

Table 1 Computed cases

case	SGS model	grid	computational domain	number of grid point	h_w	average time (Note 1)
1	S (0.13,sf_μ)*1	colocated	20 (x_1) × 14 (x_2) × 2 (x_3)	104 (x_1) × 68 (x_2) × 10 (x_2) [grid A]	0.022	≈ 61
2	DS	colocated			0.022	≈ 15
3	DM	colocated			0.022	≈ 15
4	LDM	colocated			0.022	≈ 15
5	LDM	staggered			0.022	≈ 15
6	S (0.1,mf_μ)*2	colocated	20 (x_1) × 14 (x_2) × 4 (x_3)	107 (x_1) × 103 (x_2) × 14 (x_3) [grid B]	0.02	≈ 15
7	LDM	staggered		140 (x_1) × 103 (x_2) × 32 (x_3) [grid C]	0.02	≈ 61

h_w : the grid interval adjacent to the cylinder wall
*1 S (Cs, damping function*2)
*2 sf_μ : standard Van Driest damping (=1-exp(-x_n^+/25)),
mf_μ : modified Van Driest damping (=(1-exp(-x_n^+/25)^3)$^{0.5}$)
Values are made dimensionless by the cylinder width, D, and the inflow velocity, U_0.

cases 1-5 or grid B for case 6.

A second-order centered difference scheme was adopted for the spatial derivatives. For time advancement, the second-order Adams-Bashforth scheme was used for the convection terms and the Crank-Nicolson scheme for the diffusion terms. The interval for time advancement was 1.0×10^{-3} (except 2.0×10^{-4} for cases 2 and 3) in non-dimensional time units based on U_0 and D.

At the inflow boundary, the approach flow was set to be constant and uniform and no velocity fluctuations exist. A convective condition was used at the outflow boundary of the computational domain. Symmetry conditions were employed for the lateral boundaries, and periodicity conditions were imposed for the boundary planes perpendicular to the cylinder axis. For the boundary condition at the solid walls, Werner and Wengle's approach [8] was adopted.

2. Comparison of various SGS models with grid A (cases 1-4)

Firstly, the relative performance of various SGS models, i.e., S, DS, DM and LDM, are compared using grid A (cases 1-4, cf. Table 1).

Fig.1 shows the time-averaged velocity $\langle\overline{u}_1\rangle$ along the centerline. In front of the cylinder, the results are not influenced by the difference of the SGS models used, but there are fairly large differences in the wake region. Case 1 (S model) underestimates the length of the reverse flow region considerably. Both cases 2 (DS model) and 3 (DM model) show better agreement with the experiment than does the S model, and there is little difference between the results obtained with these two types of dynamic SGS models in the region of $0.5<x_1<1.5$. Further downstream ($x_1>1.5$), case 3 (DM model) seems to give a more reasonable result than does case 2 (DS model).

Fig.2 compares the time-averaged velocity $\langle\overline{u}_1\rangle$ along the centerline between

case 3 (DM model) and case 4 (LDM model). In the LDM model, the model coefficient C ($C=Cs^2$) is calculated using the averaged quantities along the path line following the approach developed by Meneveau *et al.* [5] (eqns.(12)-(17) in the Appendix). Although both results show good agreement with the experiment, case 4 (LDM model) provides more accurate results than case 3 (DM model). The LDM model seems to provide the best result of these four SGS models. Furthermore, the use of the LDM model contributes to a remarkable improvement of calculation stability, as shown in Fig.3. Consequently, the CPU time was reduced by 33% in comparison with the DM model.

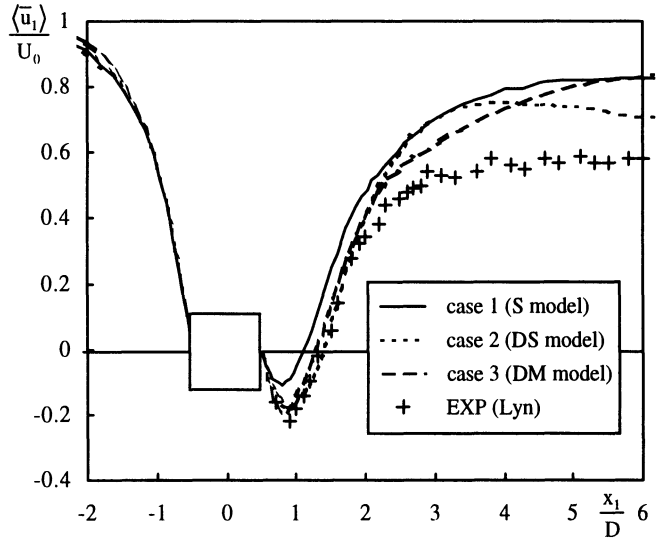

Fig.1 Comparison of the time-averaged velocity $\langle \bar{u}_1 \rangle$ along the center line for S, DS and DM models

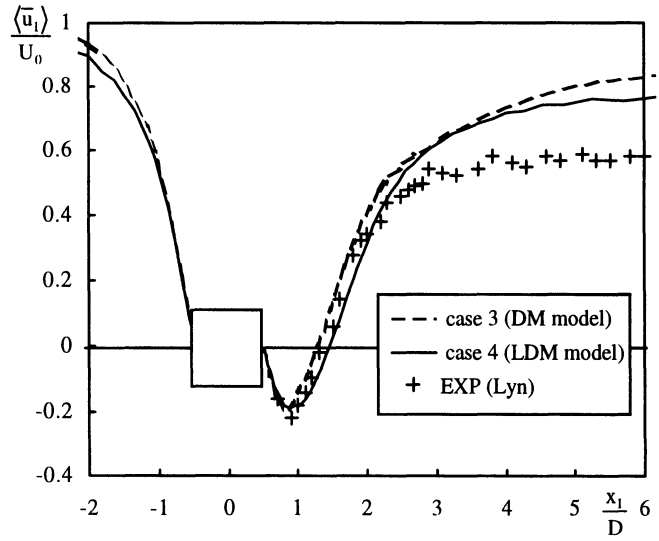

Fig.2 Comparison of the time-averaged velocity $\langle \bar{u}_1 \rangle$

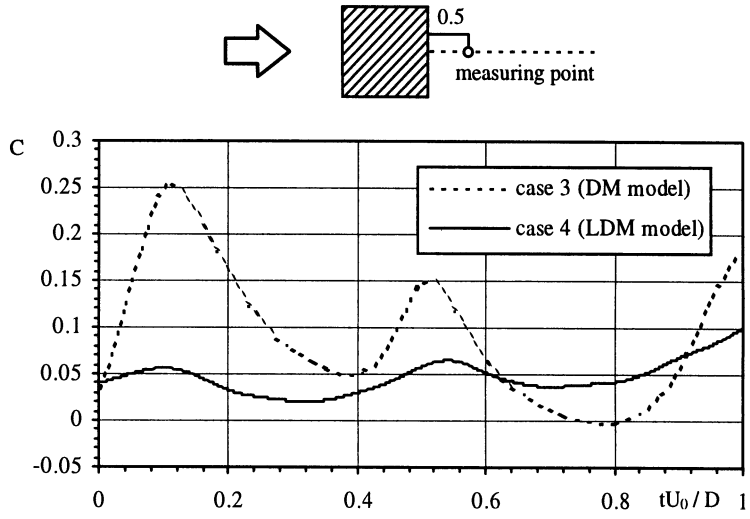

Fig.3 Comparison of the time-history of model coefficient C between DM and LDM models

3. Influence of difference in grid spacings (cases 1 and 6)

The conditions for computation (the grid spacing, SGS model, etc.) employed in case 6 are almost the same as those in the computation of UKAHY1 presented at the Rottach-Egern workshop [6].

The result of this reference case (case 6) is compared with case 1 in Fig.4. Spatial oscillation of the velocity is observed in the region of $x_1>2$ in case 6, while this oscillation does not appear in the result of case 1. As described in Note 3, this difference is mainly caused by the difference in the grid spacings for these cases. The spacing of grid B (case 6) in the streamwise (x_1) direction is coarser than that of grid A (case 1) in the region behind the cylinder ($x_1>1$). The spacing in the spanwise (x_3) direction of grid B (case 6) is also coarser than that of grid A (case 1) for the whole domain. With the coarse spacing of grid B, spatial oscillation of velocity was caused in case 6 in the region behind the cylinder, as indicated in Fig.4. On the other hand, the resolution of grid B in the x_1 and x_2 directions is finer than that of grid A in the vicinity of the cylinder wall ($-1<x_1<1$). Hence, the computation with grid B provided more accurate results in the vicinity of the cylinder wall in comparison with the results using grid A. Considering these points, a new grid (grid C) was designed. The resolution of grid C in the x_1 and x_2 directions is almost the same as that of grid B in the vicinity of the cylinder wall, but much finer than that of grid B in the region behind the cylinder. In this region, the resolution of grid C in the x_1 direction becomes identical to that of grid A. Furthermore, the grid spacing in the spanwise (x_3) direction is much finer in grid C than those in grids A or B.

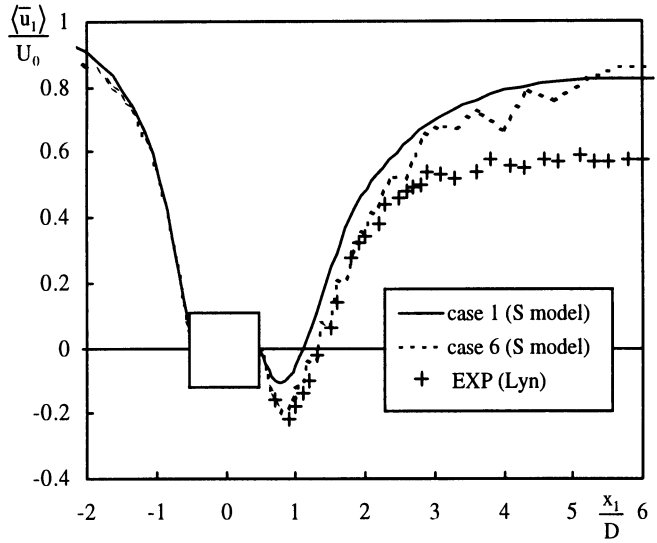

Fig.4 Comparison of the time-averaged velocity $\langle \bar{u}_1 \rangle$ along the center line between cases 1 and 6

4. Performance of LDM model with grid C (case 7)

Hereafter the results of the computation using the LDM model with grid C (case 7) are shown. In this case the staggered grid was used (Note 4). Integral parameters are compared in Table 2. The statistical quantities were determined by using the time-history of predicted flowfields during 8 vortex shedding periods for this case. The correspondence between the results of case 7 and experiments is satisfactory except for the value of C_{Drms}. Fig.5 compares the time-averaged velocity $\langle \bar{u}_1 \rangle$ along centerline. The result of case 7 reproduced the velocity distribution in the reverse flow region behind the cylinder accurately.

Table 2. Integral parameters

	$L_1 \times L_2 \times L_3$	$N_1 \times N_2 \times N_3$	h_w	St	$<C_D>$	C_{Drms}	C_{Lrms}
case 7 (LDM model)	20D × 14D × 4D	140 × 103 × 32	0.02	0.131	2.05	0.12	1.39
Lyn [7]	Experiment (Re=2.2 × 10^4)			0.132	2.1	—	—
Vickey [12]	Experiment (Re=1 × 10^5)			—	2.05	—	1.32
Lee [13]	Experiment (Re=1.76 × 10^5)			—	2.05	0.23	1.22

L_i : computational domain in x_i direction (i=1,2,3)
N_i : mesh resolution in x_i direction
St : Strouhal number
C_D : drag coefficient
C_L : lift coefficient
h_w : the grid interval in the normal direction adjacent to the cylinder wall

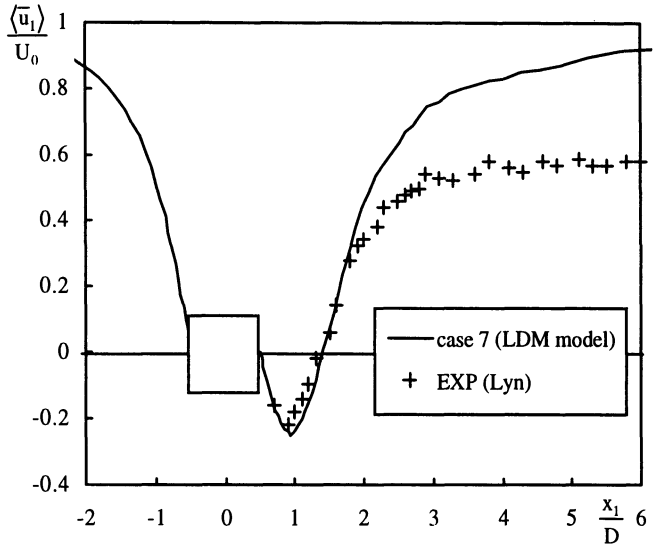

Fig.5 Comparison of the time-averaged velocity $\langle \bar{u}_1 \rangle$ along the centerline of LDM model (case 7)

5. Conclusions

(1) Dynamic SGS models provide much more accurate predictions of the sizes of the reverse flow region behind the cylinder than does the static type of conventional Smagorinsky model (S model).

(2) The method for stabilization by averaging over particle trajectories employed in the LDM model can contribute a remarkable improvement of calculation stability. In the experience of our group, the LDM model seems to be most suited for the analysis of the flowfield around a cylinder, since it provides good calculation stability and also good prediction accuracy.

Note 1

The time-averaged values were determined by the time-averaging over 8 vortex shedding periods (61 in the non-dimensional time scale) in cases 1 and 8 as well as by averaging over the spanwise direction.

Fig.6 compares the time-averaged velocity determined by time-averaging over 2 shedding periods with that averaged over 8 shedding periods for case 1 (S model). The difference between values based on these two different averaging times is very small as far as time-averaged velocity is concerned. Thus, the averaging time for time-averaged values was reduced to 2 vortex shedding periods (15 in the non-dimensional time scale) in cases 2-6.

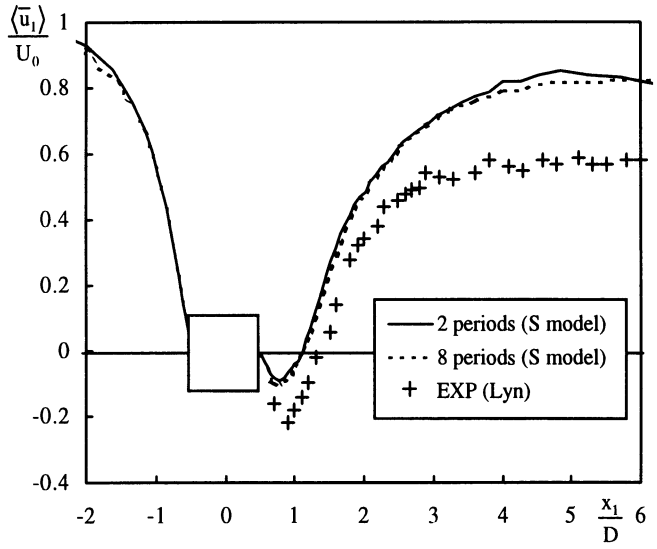

Fig.6 Comparison of the time-averaged velocity $\langle \bar{u}_1 \rangle$ along the centerline determined by time averaging over 2 shedding periods and 8 shedding periods

Note 2

In Werner and Wengle's approach [8], a linear or 1/7 power-law distribution of the instantaneous velocity is assumed :

$$\frac{\bar{u}}{u^*} = x_n^+ \qquad (x_n^+ \le 11.81),$$

$$\frac{\bar{u}}{u^*} = 8.3\, x_n^{+1/7} \qquad (x_n^+ > 11.81).$$

This wall function becomes identical to the no-slip boundary condition when $x_n^+ \le 11.81$. Fig.7 illustrates the distribution of time-averaged values of x_n^+ of the grid points adjacent to the cylinder walls. In most areas, the value of x_n^+ is lower than 11.81. Thus the linear-law, i.e., the no-slip boundary condition, is applied in these areas. At corner areas, the value of x_n^+ exceeds 11.81 a little.

Note 3

As shown in Table 1, four factors, (grid spacings, values of Cs, wall damping functions and sizes of computational domain in the spanwise direction) are different between cases 1 and 6. In the earlier research by our group (Murakami *et al.* [9]), the influence of the Cs value and the size of computational domain was examined. In that study, computations were carried out for two different values of Cs (0.13 and 0.1 adopted in cases 1 and 6 respectively) with grid A. As shown in [9], the difference between the results of these two cases was very

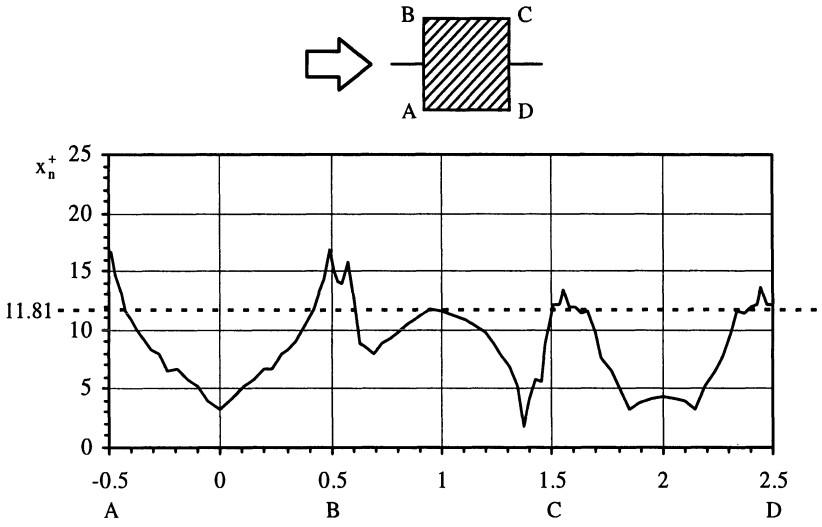

Fig.7 Distribution of time-averaged values of x_n^+ (case 7)

small. Furthermore, two computations were carried out and compared for two sizes of different computational domain in the spanwise direction, 2D and 4D, in [9]. Regarding the time-averaged velocity $\langle \overline{u}_1 \rangle$, the result of the case with a larger computational domain (4D) provided a slightly smaller reverse flow region behind the cylinder. However, we noted that there were no outstanding differences for each computational domain size.

We have also carried out another computation (case 6') in which only the damping function was changed from mf_μ $(=(1-\exp(-x_n^+/25)^3)^{0.5})$ adopted in case 6 to the function used in case 1 $(f_\mu=1-\exp(-x_n^+/25))$. Through the comparison between the results of cases 6 and 6', it was confirmed that the results were not much affected by the difference in the forms of wall damping functions.

The remaining factor that differs between cases 1 and 6 is grid spacing. We consider that the difference in the grid spacing is the main factor contributing to the differences between the results for these cases.

Note 4

A colocated grid (Rhie and Chow [10]) was used for cases 1-4 and 6. However, recently it was reported that the result based on a staggered grid provides more accurate prediction than that based on a colocated grid in a LES computation of channel flow, because the result based on colocated grid includes some numerical errors (Ooka *et al.* [11]).

In this study, we compared the result based on colocated grid (case 4) with that based on staggered grid (case 5). As for the time-averaged velocity $\langle \overline{u}_1 \rangle$, both results are almost the same, but case 5 is slightly better (figures are omitted here). So we used the staggered grid for case 7.

Nomenclature

x_i : spatial coordinates (i=1,2,3 :streamwise, lateral, spanwise)
u_i : components of the velocity vector
f : instantaneous value of a quantity, $\bar{f}$: filtered value of f,
$\langle f \rangle$: time averaged value of f
x_n : distance from the wall, $x_n^+ = x_n u^*/\nu$, u^* : friction velocity
D : width of the square cylinder,
U_0 : $\langle u_1 \rangle$ value at inflow of computational domain
Values are made dimensionless using D, U_0 and air density ρ.

References

[1] Germano,M., U.Piomelli, P.Moin and W.H.Cabot, A dynamic subgrid-scale eddy viscosity model, Phys. Fluids, A3, 1760 (1991).

[2] Lilly,D.K., A proposed modification of the Germano subgrid-scale closure method, Phys. Fluids A4, 633 (1992).

[3] Zang,Y., R.L.Street and J.R.Koseff, A dynamic mixed subgrid-scale model and its application to turbulent recirculating flows, Phys. Fluids A5 (12) pp 3186-3196 (1993).

[4] Vreman,B., B.Geurts and H.Kuerten, On the formulation of the dynamic mixed subgrid-scale model, Phys. Fluids 6 (12), pp.4057-4059 (1994).

[5] Meneveau,C., T.S.Lund and W.Cabot, A lagrangian dynamic subgrid-scale model of turbulence, Proceedings of the Summer Program 1994, Center for Turbulence Research, pp.2746-2757 (1991).

[6] LES workshop of Flows past Bluff Bodies, June 26-28 Rottach-Egern, Tegernsee, Germany, organized by W.Rodi and J.H.Ferziger (1995).

[7] Lyn, D.A., Einav S., Rodi W. and Park J.H. (1995), A laser-Doppler velocimetry study of ensemble averaged characteristics of the turbulent near wake of a square cylinder, J. Fluid Mech. vol. 304, p.285 (1995).

[8] Werner,H. and H.Wengle, Large-eddy simulation of turbulent flow over and around a cube in a plate channel, 8th Symp. on Turbulent Shear Flows 19-4 (1991).

[9] Murakami,S., W.Rodi, A.Mochida and S.Sakamoto, Large eddy simulation of turbulent vortex shedding flow past 2D square cylinders, in: Proc. Symp. on Engineering Applications of large Eddy Simulations (FED-Vol.162). ASME p.113 (1991).

[10] Rhie,C.M. and W.L.Chow, Numerical study of the turbulent flow past an airfoil with trailing edge separation, AIAA Journal, vol. 21, No.11 (1983).

[11] Ooka,R., S.Murakami and A.Mochida, Study on conservation property of kinetic energy of LES with colocated grid, submitted to International Journal of Numerical Method in Fluids.

[12] Vickery,B.J., Fluctuating lift and drag on a long cylinder of square cross section in a smooth and a turbulent stream, J. Fluid Mech. 25, p.481 (1975).

[13] Lee,B.E., The effect of turbulence on the surface pressure field of square prisms, J. Fluid Mech. 69, p.263 (1975).

[14] Bardina,J., J.H.Ferziger and W.C.Reynolds, Improved Subgrid-Scale Models for Large-Eddy Simulation, AIAA paper-80 (1981).

[15] Akselvoll,K., and P.Moin, Large eddy simulation of a backward facing step flow, Eng. Turbulence Modelling and Experiments 2 pp.303-313 (1993).

Appendix: SGS models

In the Smagorinsky model, the anisotropic part of the SGS stress τ_{ij} is modeled as follows:

$$\tau_{ij} - \frac{1}{3}\delta_{ij}\tau_{kk} = -2C\bar{\Delta}^2|\bar{S}|\bar{S}_{ij} = -2\nu_{SGS}\bar{S}_{ij} \quad (1)$$

where the SGS viscosity ν_{SGS} is

$$\nu_{SGS} = C\bar{\Delta}^2|\bar{S}| \qquad (C = Cs^2) \quad (2)$$

Here, $\bar{}$ (overbar) denotes the grid-filtered values and $\bar{\Delta}$ is the width of the grid-filter, S_{ij} is the resolved-scale strain rate tensor,

$$\bar{S}_{ij} = \frac{1}{2}\left(\frac{\partial \bar{u}_i}{\partial x_j} + \frac{\partial \bar{u}_j}{\partial x_i}\right), \quad |\bar{S}| = (2\bar{S}_{ij}\bar{S}_{ij})^{1/2} \quad (3)$$

In the S model (cases 1 and 6), C is treated as a constant. The value of 0.0169 and 0.01 were selected for cases 1 and 6, respectively. These values correspond to 0.13 and 0.1 of the so-called Smagorinsky constant Cs (cf. Table 1). $\bar{\Delta}$ is multiplied by the Van Driest wall damping function f_μ, $1\text{-}\exp(-x_n^+/25)$ in case 1 and mf_μ, $\{1\text{-}\exp(-x_n^+/25)^3\}^{0.5}$ in case 6 in order to account for the near wall effect in S model, while f_μ is not necessary in dynamic SGS models.

In dynamic SGS models, the model coefficient C is determined dynamically. Following Germano [1], a test filter (denoted as $\hat{}$) is introduced to derive an expression for C. The width of the test-filter is taken to be twice the width of the grid-filter. Germano *et al.* defined the resolved turbulent stress as follows :

$$£_{ij} = \widehat{\bar{u}_i\bar{u}_j} - \hat{\bar{u}}_i\hat{\bar{u}}_j \quad (4)$$

$£_{ij}$ can be related to the SGS stress τ_{ij} and the subtest stress $T_{ij} = \widehat{u_i u_j} - \hat{\bar{u}}_i\hat{\bar{u}}_j$ by

$$£_{ij} = T_{ij} - \hat{\tau}_{ij} \quad (5)$$

The DS model (case 2) employs the dynamic procedure using a least square method proposed by Lilly [2] to determine the coefficient C :

$$C(\vec{x}, t) = -\frac{1}{2}\frac{£_{ij}M_{ij}}{M_{kl}^2} \quad (6)$$

$$\text{where } M_{ij} = \hat{\bar{\Delta}}^2\left|\hat{\bar{S}}\right|\hat{\bar{S}}_{ij} - \widehat{\bar{\Delta}^2|\bar{S}|\bar{S}_{ij}} \quad (7)$$

In DM model (case 3) a linear combination of the dynamic Smagorinsky model and the scale similarity model is adopted [4, 14]. In the DM model, the anisotropic part of τ_{ij} is expressed as [4, 14] :

$$\tau_{ij} - \frac{1}{3}\delta_{ij}\tau_{kk} = -2\nu_{SGS}\bar{S}_{ij} + B_{ij} - \frac{1}{3}\delta_{ij}B_{kk} \quad (8)$$

$$\text{where } B_{ij} = \overline{\bar{u}_i\bar{u}_j} - \bar{\bar{u}}_i\bar{\bar{u}}_j \quad (9)$$

The first and the second terms on the right-hand of eqn.(8) derive from the

Smagorinsky and the scale similarity models respectively. C is determined by

$$C(\vec{x},t) = -\frac{1}{2}\frac{M_{ij}(\pounds_{ij} - H_{ij})}{M_{kl}^2} \tag{10}$$

where H_{ij} is the term originating from the scale similarity model, written as [4] ;

$$H_{ij} = \widehat{\hat{\bar{u}}_i \hat{\bar{u}}_j} - \hat{\bar{u}}_i \hat{\bar{u}}_j - (\widehat{\bar{u}_i \bar{u}_j} - \bar{u}_i \bar{u}_j) \tag{11}$$

The value of C obtained from eqns.(6) and (10) can be either positive or negative. A negative value of C implies a locally negative value of eddy-viscosity which causes the numerical instability. In cases 2 and 3, we set the coefficient C equal to zero wherever C was estimated to be negative (clipping procedure).

Previous authors have used averaging over homogeneous directions to avoid the numerical instability (Germano *et al.* [1], Akselvoll *et al.* [15], Zang *et al.* [3]). The disadvantages of this treatment is that the plane-averaging can only be applied to flowfields that have a homogeneous direction. This treatment cannot be applied to three-dimensional flowfields such as a flow around a cube; thus this treatment excludes the application of LES to more challenging flows of engineering interest. In the Lagrangian Dynamic Smagorinsky model (LDS model), the model coefficient C is calculated following the approach developed by Meneveau *et al.* [5] in which the residual in eqn.(5) is minimized along fluid trajectories rather than flow homogeneous directions, resulting in an expression for the model coefficient :

$$C(\vec{x},t) = -\frac{1}{2}\frac{I_{LM}}{I_{MM}} \tag{12}$$

The numerator and denominator of eqn.(12) are obtained using a simple time discretization, resulting in

$$I_{LM}^{n+1}(\vec{x}) = H\left\{\varepsilon \pounds_{ij}^{n+1} M_{ij}^{n+1}(\vec{x}) + (1-\varepsilon) I_{LM}^{n}(\vec{x} - \bar{u}_i^{\,n}\Delta t)\right\} \tag{13}$$

$$I_{MM}^{n+1}(\vec{x}) = \varepsilon M_{ij}^{n+1} M_{ij}^{n+1}(\vec{x}) + (1-\varepsilon) I_{MM}^{n}(\vec{x} - \bar{u}_i^{\,n}\Delta t) \tag{14}$$

where H{x} is the ramp function (H{x}=x if x>0 and zero otherwise), and

$$\varepsilon = \frac{\Delta t / T^n}{(1 + \Delta t / T^n)} \tag{15}$$

The technique of Lagrangian averaging can be easily added to the Dynamic Mixed model. We call it the LDM model.

$$C(\vec{x},t) = -\frac{1}{2}\frac{I_{LM} - I_{HM}}{I_{MM}} \tag{16}$$

$$\text{where } I_{HM}^{n+1}(\vec{x}) = \varepsilon H_{ij}^{n+1} M_{ij}^{n+1}(\vec{x}) + (1-\varepsilon) I_{HM}^{n}(\vec{x} - \bar{u}_i^{\,n}\Delta t) \tag{17}$$

The LDM model was used in cases 4, 5 and 7 in Table 1.

The time-scale T in eqn.(15) is defined as $T=\alpha n$ ($n=\bar{\Delta}\, I_{LM}^{-1/4}$). Meneveau *et al.* [5] recommend a value of 2 for α based on the filtered DNS data of isotropic turbulence. In the experience of our group, this value of 2 was not optimum for α for flow around a bluff body. Here, the value of 0.2 was selected for α ($T=0.2n$) in cases 4, 5 and 7 as a result of numerical experiments.

LES OF FLOW OVER A SQUARE CYLINDER

G. WANG AND S.P. VANKA
Department of Mechanical and Industrial Engineering
University of Illinois at Urbana-Champaign, IL 61801, USA

Abstract. In the present study we have performed LES of flow over a square cylinder at a Reynolds number of 21,400. Several calculations with progressive improvements in numerical accuracy and grid resolution have been conducted, and the results from one of these are included in the test case exercise.

1. Introduction

The problem considered is the flow over a square cylinder that is placed normal to a uniform free stream. We present the results of one of several Large-Eddy Simulations of high Reynolds number turbulent flow over the square cylinder.

In the following sections, we provide details of the numerical schemes use in our study and of the implementation of the dynamic subgrid-scale model. A full report of the various simulations performed is given by Wang and Vanka (1996).

2. Governing Equations

In large eddy simulations, the resolved flow field is separated from the sub-grid field by applying a spatial filter to a continuous function in space and time. After applying a suitable filter to the continuity and momentum equations, the filtered equations of motion can be written as :

$$\frac{\partial \overline{u}_i}{\partial x_i} = 0 \tag{1}$$

$$\frac{\partial \overline{u}_i}{\partial t} + \frac{\partial}{\partial x_j}(\overline{u}_i \overline{u}_j) = -\frac{\partial \overline{p}}{\partial x_i} - \frac{\partial \tau_{ij}}{\partial x_j} + \frac{1}{Re}\frac{\partial^2 \overline{u}_i}{\partial x_j \partial x_j} \tag{2}$$

J.-P. Chollet et al. (eds.), Direct and Large-Eddy Simulation II, 397-400.

where the index $i = 1, 2, 3$ refers to the streamwise (x-direction), crosswise (y-direction) and spanwise (z-direction) directions, respectively. In the above equations, the velocities are non-dimensionalized by the freestream velocity, U_0, and the pressure is non-dimensionalized by the inlet dynamic pressure, $\rho {U_0}^2$.

The subgrid-scale stress τ_{ij} in equation (2) represents the effects of small scales, and must be modeled. The key to success in large eddy simulations is the accurate representation of the unresolved subgrid-scale motions. In the Smagorinsky model the subgrid stresses are related to the resolved strain rates through an isotropic viscosity, ν_T. Thus,

$$\tau_{ij} - \frac{\delta_{ij}}{3}\tau_{kk} = -2\nu_T \overline{S}_{ij} \tag{3}$$

where δ_{ij} is the Kronecker delta. The eddy viscosity, ν_T, and the large scale strain rate tensor, $\overline{S}_{ij}$, are defined as

$$\nu_T = C_s \overline{\Delta}^2 \sqrt{2\overline{S}_{ij}\overline{S}_{ij}} = C_s \overline{\Delta}^2 |\overline{S}| \tag{4}$$

$$\overline{S}_{ij} = \frac{1}{2}\left(\frac{\partial \overline{u}_i}{\partial x_j} + \frac{\partial \overline{u}_j}{\partial x_i}\right) \tag{5}$$

C_s is the dimensionless model coefficient, $\overline{\Delta} = (\Delta x \Delta y \Delta z)^{1/3}$ is the grid filter width. In the dynamic model, the value of the C_s coefficient is calculated at every time step, as the flow evolves, by examining the instantaneous energy transfers. A second filter, called the test filter (denoted by $\hat{}$), is applied to the resolved velocity field and the resolved turbulent stresses, $\mathcal{L}_{ij}$, the subgrid scale stresses, τ_{ij}, and the subtest-scale stresses are related to determine the coefficient C_s. We currently use the modification proposed by Lilly (1992) to the original Germano model (1991) which provides the following expression for C_s.

$$C_s = -\frac{1}{2}\frac{< \mathcal{L}_{ij}\mathcal{M}_{ij} >}{< \mathcal{M}_{ij}\mathcal{M}_{ij} >} \tag{6}$$

where $<>$ denotes averaging in the spanwise direction. $\mathcal{L}_{ij}$ and $\mathcal{M}_{ij}$ are defined as :

$$\mathcal{L}_{ij} = \widehat{\overline{u}_i \overline{u}_j} - \hat{\overline{u}}_i \hat{\overline{u}}_j \tag{7}$$

$$\mathcal{M}_{ij} = \hat{\overline{\Delta}}^2 |\hat{\overline{S}}| \hat{\overline{S}}_{ij} - \overline{\Delta}^2 \widehat{|\overline{S}| \overline{S}_{ij}} \tag{8}$$

The test filter has been applied only in the spanwise (homogeneous) direction. Thus, $\hat{\overline{\Delta}}/\overline{\Delta}$, which is the ratio of the filter widths, is $2^{1/3}$ according

to the definition of $\Delta = (\Delta x \Delta y \Delta z)^{1/3}$. Further, negative C_s is truncated to ensure that the total viscosity $(\nu + \nu_T)$ remained positive.

3. Numerical Procedure

The above equations are numerically integrated in time by a two-stage fractional step procedure with Adams-Bashforth explicit differencing for both convection and diffusion terms.

$$\frac{\tilde{u_i} - {u_i}^n}{\Delta t} = \frac{3}{2} H_i^n - \frac{1}{2} H_i^{n-1} \tag{9}$$

$$\nabla \cdot (\nabla p) = \frac{1}{\Delta t} \frac{\partial \tilde{u_i}}{\partial x_i} \tag{10}$$

$$u_i^{n+1} = \tilde{u_i} - \frac{\partial p}{\partial x_i} \Delta t \tag{11}$$

where $\tilde{u_i}$ is the intermediate velocity field, and H_i is given by

$$H_i = -\frac{\partial}{\partial x_j}(u_i u_j) - \frac{\partial \tau_{ij}}{\partial x_j} + \frac{1}{Re} \frac{\partial^2 u_i}{\partial x_j \partial x_j} \tag{12}$$

A collocated arrangement has been used for the velocities and pressure and the spatial derivatives are integrated with a finite-volume methodology. The values at the cell faces are evaluated with either third-, fifth-, or seventh-order accuracy for the convection terms and second-, fourth- or sixth-order accuracy for the diffusion terms.

The above equations are solved on a grid which may in general be curvilinear in the $x - y$ plane. Volume fluxes at the cell faces are given by the relation :

$$U = J(\xi_x u + \xi_y v) \tag{13}$$

$$V = J(\eta_x u + \eta_y v) \tag{14}$$

$$W = J(\gamma_z w) \tag{15}$$

where ξ_x, ξ_y, η_x, η_y, and γ_z are the metrics and J is the Jacobian of transformation. The volume fluxes at the cell faces are required to satisfy the continuity equation.

The pressure is computed from the pressure Poisson equation. The solution of the pressure equation on a general curvilinear grid requires an iterative procedure, and the same conjugate gradient method was used in the present computations on a Cartesian mesh. In order to enforce mass conservation, the Poisson equation for pressure was discretized using the finite-volume approach. In the computational space, the equation is integrated over a cell volume centered at the collocation point. Computation of

the pressure is the most computationally intensive operation of the entire algorithm. The convergence rate of the iterative solver can be accelerated by the utilization of a preconditioner with the conjugate gradient method. In the present algorithm, provision is made to perform several Jacobi iterations alternating with every CG iteration to accelerate the convergence.

4. Simulation Results

The results from a single LES (Run 4 of Wang and Vanka (1996)) are included in this test case exercise. This run utilised a total of $192 \times 160 \times 48$ grid points on a domain extending from $-8d$ to $16d$ in the streamwise direction, from $-10d$ to $10d$ in the crosswise direction, and of dimension πd in the spanwise direction. This simulation used fifth-order differencing for the convection terms and fourth-order differencing for the diffusion terms. The time step was 2×10^{-3} and statistics were gathered over 11 shedding cycles (60000 time steps).

Selected results are given in the preceding review paper in this volume by Voke. For detailed comparisons of all the simulations in the study, see Wang and Vanka (1996) and Wang (1996).

References

GERMANO, M. PIOMELLI, U., MOIN, P. and CABOT, W. (1991) A dynamic subgrid-scale eddy viscosity model, *Phys Fluids A*, **3**, p. 1760.

LILLY, D.K. (1992) A proposed modification of the Germano subgrid-scale closure method, *Phys Fluids A*, **4**, p. 633.

WANG G. and VANKA, S.P. (1996) Large eddy simulations of high Reynolds number flow over a square cylinder, Report CFD 96-02, Computational Fluid Dynamics Laboratory, Dept. Mech. and Ind. Eng., University of Illinios at Urbana-Champaign, IL 61801.

WANG, G. (1996) Large eddy simulations of turbulent flow over a square cylinder on a massively parallel computer, *Ph.D. Dissertation* (in preparation) Dept. Mech. and Ind. Eng., University of Illinios at Urbana-Champaign.

LES OF FLOW AROUND A SQUARE CYLINDER

TETSUYA KOGAKI
Graduate School, University of Tokyo
7-3-1 Hongou, Bunkyo-ku, 113 Tokyo, Japan

AND

TOSHIO KOBAYASHI AND NOBUYUKI TANIGUCHI
Institute of Industrial Science, University of Tokyo
7-22-1 Roppongi, Minato-ku, 106 Tokyo, Japan

Abstract.

Large-eddy simulations (LES) of turbulent flow around a square cylinder at Reynolds number of 2.2×10^4 are conducted. The subgrid-scale (SGS) models used here are the standard Smagorinsky model and a dynamic mixed SGS model. Simulation results indicate that the spanwise flow structure behind the cylinder is highly influenced by the spanwise mesh resolution and that the artificial dissipative effects of upwind schemes cannot be ignored even in the case of higher order upwind schemes.

1. SGS model

The standard Smagorinsky model (Smagorinsky, 1963; Deardorff, 1970) is expressed as follows:

$$\tau_{ij} - \frac{1}{3}\delta_{ij}\tau_{kk} = -2\left(C_s\overline{\Delta}\right)^2 \left|\overline{S}\right| \overline{S}_{ij}, \tag{1}$$

$$\overline{S}_{ij} = \frac{1}{2}\left(\frac{\partial \overline{u}_i}{\partial x_j} + \frac{\partial \overline{u}_j}{\partial x_i}\right), \quad |S| = \sqrt{2\overline{S}_{ij}\overline{S}_{ij}}, \tag{2}$$

where the value of the model coefficient is C_S set to be 0.13, which is conjectured by Mochida *et al.* (1993).

On the other hand, the model coefficient is computed dynamically in a dynamic SGS model (DSM) (Germano *et al.*, 1991). Zang *et al.* (1993) modified the DSM by incorporation of the mixed model of Bardina *et al.*

J.-P. Chollet et al. (eds.), Direct and Large-Eddy Simulation II, 401-408.

(1983). Moreover, Vreman *et al.* (1994) rewrote the dynamic mixed SGS model in order to remove a mathematical inconsistency (hereafter the dynamic version of mixed model developed by Vreman *et al.* is referred to as DMSM). SGS stresses of the DMSM are given by

$$\tau_{ij} - \frac{1}{3}\delta_{ij}\tau_{kk} = -2C\overline{\Delta}^2 \left|\overline{S}\right| \overline{S}_{ij} + L^m_{ij} - \frac{1}{3}\delta_{ij}L^m_{kk} , \tag{3}$$

where L^m_{ij} is the modified Leonard term represented by

$$L^m_{ij} = \overline{\overline{u}_i\overline{u}_j} - \overline{\overline{u}}_i\overline{\overline{u}}_j . \tag{4}$$

Using the least-square approach suggested by Lilly (1992), the model coefficient C of DMSM is computed as

$$C = -\frac{1}{2}\frac{\langle (L_{ij} - H_{ij})\, M_{ij}\rangle}{\langle M_{ij}M_{ij}\rangle} , \tag{5}$$

$$L_{ij} = \widetilde{\overline{u}_i\overline{u}_j} - \tilde{\overline{u}}_i\tilde{\overline{u}}_j , \tag{6}$$

$$H_{ij} = \widetilde{\tilde{\overline{u}}_i\tilde{\overline{u}}_j} - \tilde{\tilde{\overline{u}}}_i\tilde{\tilde{\overline{u}}}_j - \left(\widetilde{\overline{\overline{u}_i\overline{u}_j}} - \widetilde{\overline{\overline{u}}_i\overline{\overline{u}}_j}\right) , \tag{7}$$

$$M_{ij} = \overline{\Delta}^2 \left(\alpha^2 \left|\tilde{\overline{S}}\right| \tilde{\overline{S}}_{ij} - \widetilde{\left|\overline{S}\right| \overline{S}_{ij}}\right) , \quad \alpha = \tilde{\overline{\Delta}}/\overline{\Delta} , \tag{8}$$

where brackets '$\langle\rangle$' in eq. (5) denote averaging operations in homogeneous directions.

The dynamic versions of the SGS model require an explicit filter operation. The test-scale filtering and the grid-scale filtering with the top-hat filter or the Gaussian filter are evaluated using Simpson's rule as follows:

$$\tilde{\overline{f}} = \overline{f} + \frac{\tilde{\Delta}^2}{24}\cdot\nabla^2\overline{f} + \mathrm{O}\left(\tilde{\Delta}^4\right) , \tag{9}$$

$$\overline{\overline{f}} = \overline{f} + \frac{\overline{\Delta}^2}{24}\cdot\nabla^2\overline{f} + O\left(\overline{\Delta}^4\right) . \tag{10}$$

2. Methods

2.1. RESOLUTION

The computational domain, total numbers of node points and SGS models used in our computation are given in Table 1. The computational domain is the same one prescribed by the organizer except for the length from the

TABLE 1. Mesh Configurations

Case	Domain	Resolution	SGS model
IS1	21.1D×14.0D×4.0D	76,880 (82×63×16)	Smagorinsky
IS2	21.1D×14.0D×4.0D	153,760 (82×63×32)	Smagorinsky
IS3	20.4D×14.0D×4.0D	347,648 (112×104×32)	DMSM

center of the cylinder to the outlet, which is extended up to more than $20D$ (D = side of the cylinder). The mesh used in case IS3 has the same resolution in the (x,y)-plane as the mesh used by the University of Karlsruhe group (UK1).

2.2. NUMERICAL METHODS

The finite volume method (FVM) was employed and the coupling scheme between the continuity equation and the pressure was based on the HSMAC method proposed by Hirt *et al.* (1972). The second order upwind scheme QUICK for the convection terms and second order central differencing for the diffusion terms were used for case IS1 and IS2. A combination of the fifth order upwind scheme (Rai and Moin, 1991) and fourth order central differencing was used for case IS3. The time marching method was a semi-implicit method with the second order Adams-Bashforth method for the convection terms and the Crank-Nicolson scheme for the diffusion terms. To stabilize the dynamic mixed model, the model coefficient C was averaged in the spanwise direction and the total viscosity was clipped to be non-negative. Moreover, in laminar flow regions where M_{ij} becomes almost zero, the model coefficient became excessively large. Therefore, we set $C = 0$ wherever $M_{ij} \times M_{ij}$ is less than 10^{-6} (Mochida *et al.*, 1995).

2.3. BOUNDARY CONDITIONS

A no-slip condition was adopted on the surface of the cylinder, while free slip conditions were used on the top and bottom domain boundaries. At the entrance to the flow domain, a constant velocity with no perturbations was imposed. At the exit of the flow domain, a convective boundary condition was used (Pauley *et al.*, 1990; Dai *et al.*, 1992):

$$\frac{\partial \overline{u}_i}{\partial t} + U_C \frac{\partial \overline{u}_i}{\partial x_1} = 0 \,, \tag{11}$$

where U_C is the convection velocity which we set equal to the mean velocity at the entrance. The spanwise boundary condition was periodic.

3. Results

Contours of the instantaneous streamwise component of the vorticity vector q_x in the (x,z)-plane at the centerline are compared between the three cases in figure 1. Comparing IS1 and IS2, it is found that the size of the streamwise vortices behind the cylinder is highly affected by the number of node points in the spanwise direction. In the case of the flow around a circular cylinder, the mean spacing of the streamwise vortex pairs behind the cylinder observed experimentally was approximately one cylinder diameter over the wide range of Reynolds number 320 to 21,000 (Bays-Muchmore *et al.*, 1993). It is expected that the spanwise mesh resolution for IS1 was not sufficient to resolve the appropriate spanwise structure. The spanwise flow structures for case IS3 have the same tendency as the case IS2 near the cylinder up to $x \cong 2$; however the arrangement of the streamwise vortex pairs becomes unstable in the far wake region.

To evaluate the effects of the upwind schemes at the scalar level (Clark *et al.*, 1979), the GS energy equation with additional artificial terms in the upwind schemes is considered:

$$\frac{\partial}{\partial t}\left(\frac{1}{2}\overline{u}_i\overline{u}_i\right)+\overline{u}_j\frac{\partial}{\partial x_j}\left(\frac{1}{2}\overline{u}_i\overline{u}_i\right)=\frac{\partial}{\partial x_j}\left(T_{ij}\overline{u}_i\right)-\frac{2}{Re}\overline{S}_{ij}\overline{S}_{ij}+\tau_{ij}\overline{S}_{ij}+E\ , \quad (12)$$

where

$$T_{ij}=-\overline{p}\delta_{ij}+\frac{2}{Re}\overline{S}_{ij}-\tau_{ij}\ . \quad (13)$$

The second and third terms on the right-hand side of eq. (12) are the molecular viscous dissipation and the turbulent viscous dissipation evaluated by the SGS models, respectively. The artificial additional terms of QUICK and of the fifth order upwind scheme are given by

$$E=-\overline{u}_i\overline{u}_j\frac{\Delta x_j^2}{24}\frac{\partial^3\overline{u}_i}{\partial x_j^3}-\overline{u}_i\left|\overline{u}_j\right|\frac{\Delta x_j^3}{16}\frac{\partial^4\overline{u}_i}{\partial x_j^4}\qquad\text{(QUICK)}\ , \quad (14)$$

$$E=\overline{u}_i\left|\overline{u}_j\right|\frac{\Delta x_j^5}{60}\frac{\partial^6\overline{u}_i}{\partial x_j^6}\qquad\text{(5th order upwind scheme)}\ . \quad (15)$$

The additional artificial terms of QUICK have dispersive and dissipative effects on the numerical solution while the fifth order upwind scheme has only dissipative effects.

Figure 2 shows distributions of the instantaneous values of the additional artificial terms of QUICK compared with the total viscous dissipation in the GS energy eq. (12) for IS2. In the vicinity of the cylinder and the near wake region, the dissipative effect of QUICK is larger than the

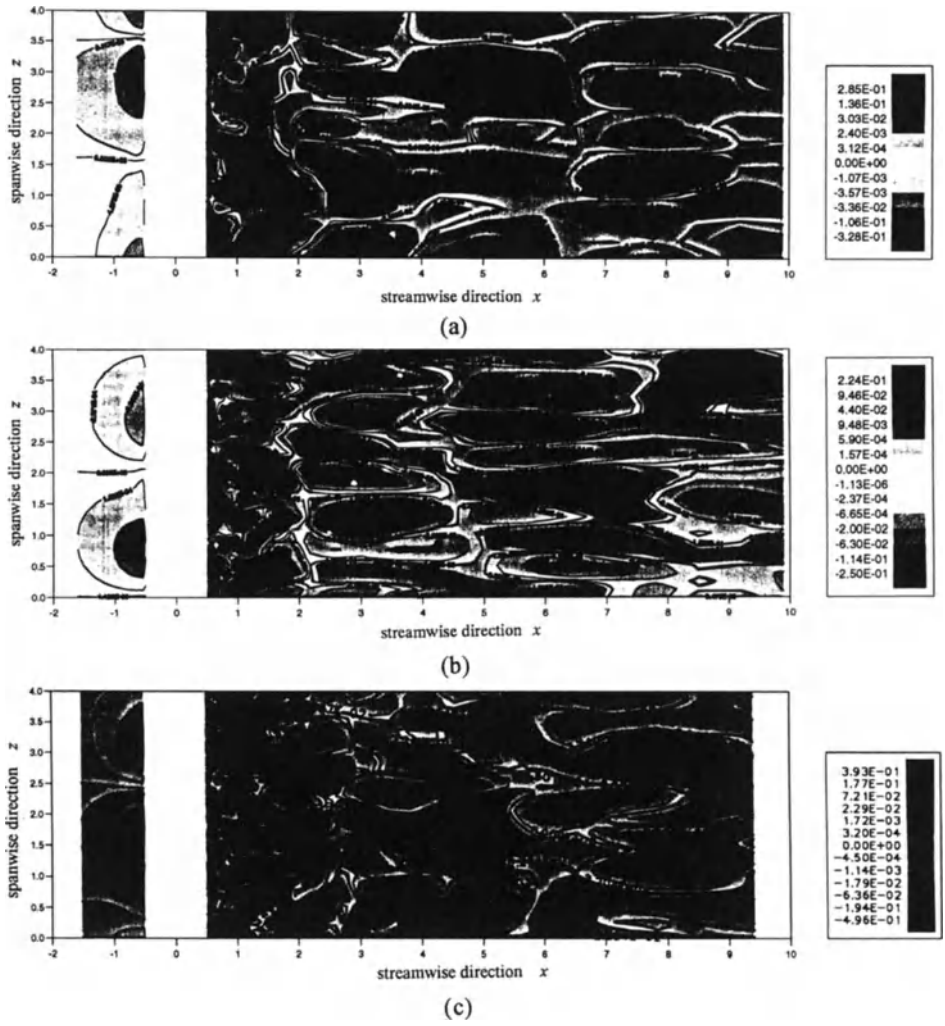

Figure 1. Contours of the streamwise component of the vorticity vector q_x in the (x,z)-plane at the centerline. (a) IS1; (b) IS2; (c) IS3.

total viscous dissipation. In the case of the fifth order upwind scheme (figure 3), the region that exhibits high values of the additional artificial terms becomes small but the maximum values was comparable to that of QUICK ($E_{max} \cong 4 \times 10^{-1}$ for both cases of QUICK and the 5th order upwind scheme in the wake region).

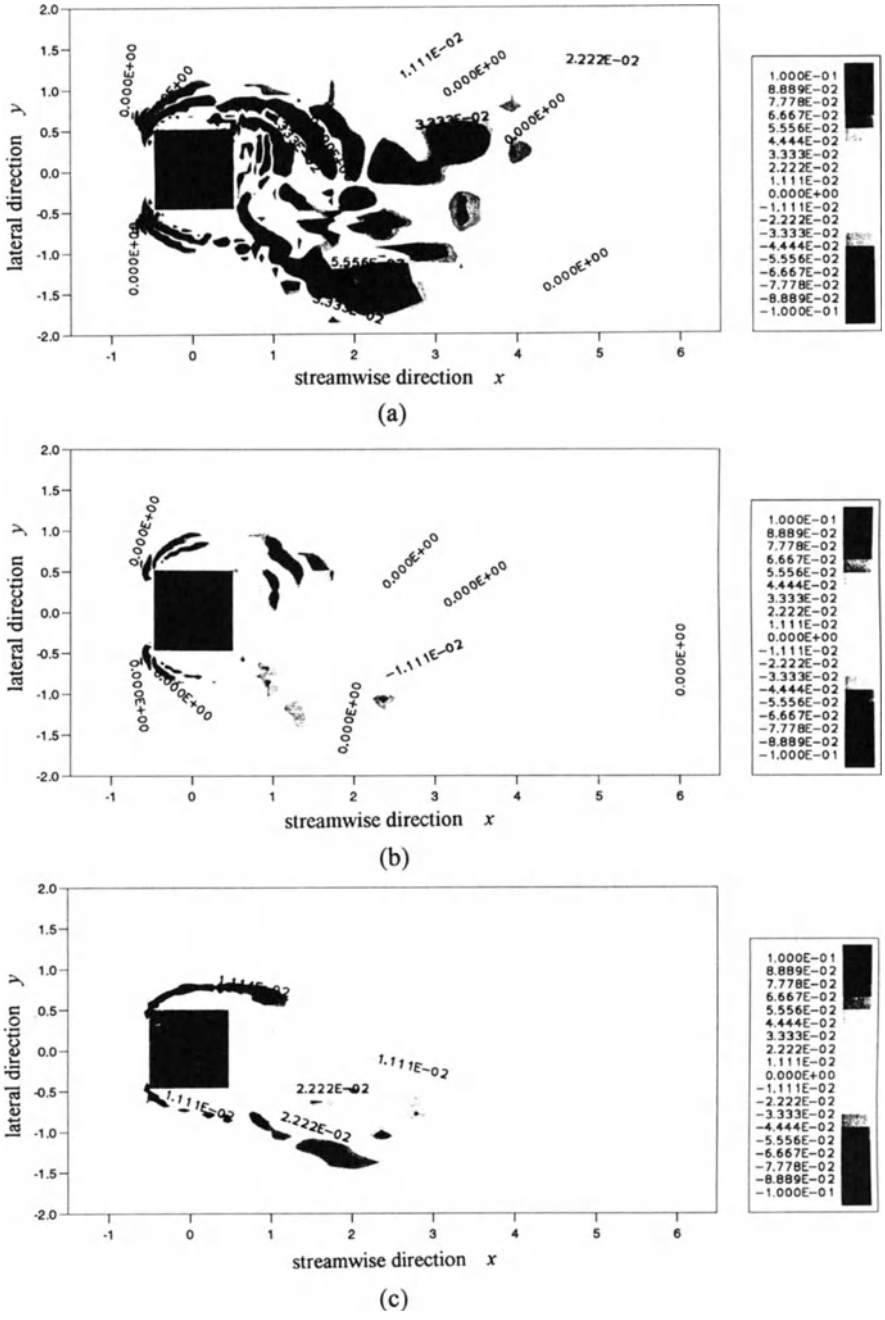

Figure 2. The distribution of the instantaneous values of the additional artificial terms of QUICK and the total viscous dissipation in the GS energy equation for IS2: (a) dissipative term; (b) dispersive term ; (c) total viscous dissipation.

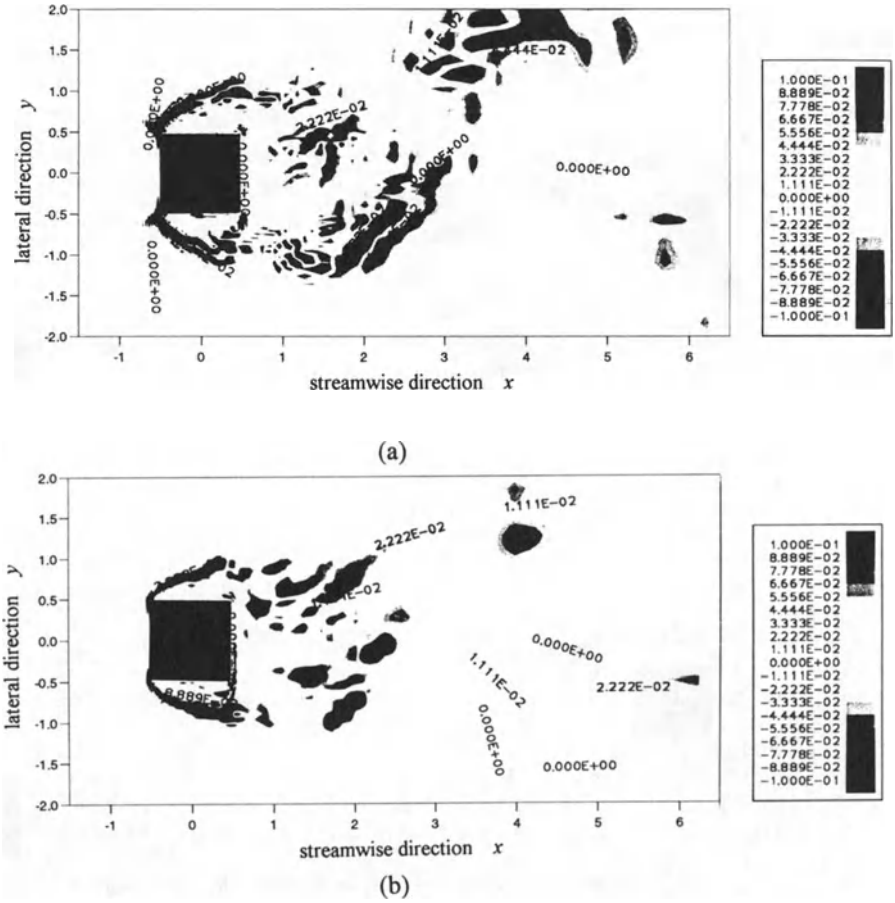

Figure 3. The distribution of the instantaneous values of the artificial additional term of the fifth order upwind scheme and the total viscous dissipation in the GS energy equation for IS3: (a) dissipative term; (b) total viscous dissipation.

4. Discussions and Conclusions

The effect of the spanwise mesh resolution was investigated using computational grids that have the same mesh resolution in the (x, y)-plane. The spanwise flow structure is highly affected by the number of spanwise node points; therefore more than 10 node points in the spanwise direction per cylinder length is appropriate to capture the proper spanwise structure.

Moreover, the qualitative effect of introducing upwind schemes for the convection terms was investigated in the GS energy equation. In the case of the second order upwind scheme QUICK (IS1 and IS2), the artificial dissipative effect due to the upwinding was larger than that of the Smagorinsky model. Therefore, the SGS model was covered by the upwinding. To reduce the effect of upwinding, the fifth order upwind scheme of Rai and Moin and a finer mesh resolution in the (x, y)-plane was adopted in case IS3.

The effect of the upwind scheme could not be ignored even in this case in the instantaneous GS energy equation. However, the profile of the time-averaged velocity and turbulence intensities were in fairly good agreement with the experimental data (Lyn, 1994) in all the cases. Therefore, in engineering terms, it is too early to conclude that the use of the upwind scheme is purposeless.

References

Bardina, J., Ferziger, J. H. and Reynolds, W. C., Improved turbulence models based on large eddy simulation of homogeneous incompressible turbulent flows, *Ph.D. dissertation*, Dept Mech. Eng. (1983), Stanford University

Bays-Muchmore, B and Ahmed, A., On streamwise vortices in turbulent wakes of cylinders, *Phys. Fluids* A**5** (1993) 387–392.

Clark, R. A., Ferziger, J. H. and Reynolds, W. C., Evaluation of subgrid-scale models using an accurately simulated turbulent flow,*J. Fluid Mech.* **91** (1979) 1–16.

Dai, Y. and Kobayashi, T., Numerical analysis on outflow boundary condition of vortex convection with uniform mean flow, *Trans. of JSME* **58-546** B(1992, in Japanese), 313–320.

Deardorff, J. W., A numerical study of three-dimensional turbulent channel flow at large Reynolds numbers, *J. Fluid Mech.* **41** (1970), 453–480.

Germano, M., Piomelli, U., Moin, P., and Cabot W. H., A dynamic subgrid-scale eddy viscosity model, *Phys. Fluids* **A3** (1993), 1760–1765

Hirt, C. W. and Cook, J. L., Calculating three-dimensional flows around structures and over rough terrain, *J. Comput. Phys.* **10** (1972), 324–340.

Kogaki, T., Kobayashi, T. and Taniguchi, N., Large eddy simulation of flow around a rectangular cylinder, submitted to *Special Issue on Mathematical Modeling of Turbulent Flows* (ed. Daiguji *et al.*, Elsevier).

Lilly, D. K., A proposed modification of the Germano subgrid-scale closure method, *Phys. Fluids* **A4** (1992), 663–635

Lyn, D. A., Einav, S., Rodi, W. and Park, J. H. A laser-Doppler velocimetry study of ensemble-averaged characteristics of the turbulent near wake of a square cylinder, *Rept. SFB* **210/E/100** (1994).

Mochida, A., Murakami, S., Rodi, W. and Sakamoto, S., Large eddy simulation of vortex shedding flow past 2D square cylinder, *J. Wind Eng.* **55** (1993, in Japanese), 79–80.

Mochida, A., Murakami, S. and Tominaga, Y., Large eddy simulation of flow past 2D square cylinder using dynamic mixed SGS model, *Seisan-Kenkyu (Mon. J. Institute of Industrial Science, University of Tokyo)* **47** (1995, in Japanese), 79–84

Pauley, L. L., Moin, P. and Reynolds, W. C., The structure of two-dimensional separation, *J. Fluid Mech.* **220** (1990), 397–411.

Rai, M. M. and Moin, P., Direct Simulations of Turbulent Flow Using Finite-Difference Schemes, *J. Comput. Phys.* **96** (1991), 15–53

Smagorinsky, J., General circulation experiments with the primitive equations. I. The basic experiment, *Mon. Weath. Rev.* **91** (1963), 99–164.

Taniguchi, N., Dynamic SGS model by finite difference method, *Seisan-Kenkyu (Mon. J. Institute of Industrial Science, University of Tokyo)* **47** (1995, in Japanese), 120–123

Vreman, B, Geurts, B. and Kuerten, H., On the formulation of the dynamic mixed subgrid-scale model, *Phys. Fluids* **6** (1994), 4057–4059

Zang, Y., Street, R. L. and Koseff, J. R. A dynamic mixed subgrid-scale model and its application to turbulent recirculating flows, *Phys. Fluids* A**5** (1993), 3186–3196.

LES OF FLOW PAST A SQUARE CYLINDER USING EMBEDDED MESHES

KOJIRO NOZAWA
Izumi Research Institute, Shimizu Corporation
2-2-2, Uchisaiwai-cho, Chiyoda-ku, Tokyo 100, Japan

AND

TETSURO TAMURA
Tokyo Institute of Technology,
4259, Nagatsuta-cho, Midori-ku, Yokohama-shi,
Kanagawa 226, Japan

1. Introduction

This paper presents the result of a large-eddy simulation of the complicated turbulent flow past a square cylinder. The technique of embedded meshes is employed for the computation of turbulent flows with various scales. We also apply the 3rd-order upwind scheme (Kawamura *et al.*, 1984) to the convective terms to avoid numerical instability.

In the flow past a bluff cylinder, there is a large area of high shear rate which it must be very expensive to cover with a fine mesh. Without using any stabilizing technique, we can hardly avoid numerical instability. However, using a high-order upwind scheme to avoid numerical instability, there will be excess damping in the area where the flow is turbulent and the subgrid viscosity of LES must work, if the mesh is not sufficiently fine.

Figure 1 shows the results of LES for the Re_τ=180 turbulent channel flow in which a 3rd-order upwind scheme is applied and the subgrid-scale eddy viscosity is generated by a dynamic procedure. In the simulation, by using a larger width filter of $2h$ or $4h$ (h is grid size) for LES instead of $1h$ and reducing the coefficient of the numerical dissipation terms of the 3rd-order upwind scheme, it becomes closer to the DNS results. This means it is possible to suppress the numerical effects through the choice of the filter width.

J.-P. Chollet et al. (eds.), Direct and Large-Eddy Simulation II, 409-412.

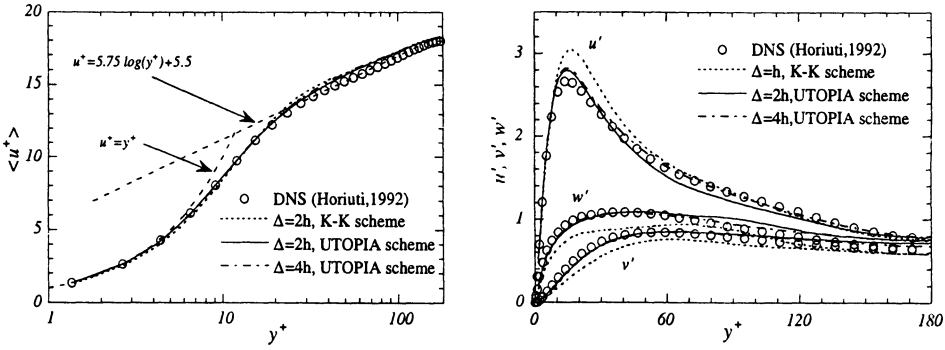

Figure 1. Re_τ=180 channel flows: left, mean-velocity profiles; right, root-mean-square velocity fluctuations normalized by the wall shear velocity.

Accordingly in the present calculation we refine the mesh by using embedded meshes and make the filter width to be double the grid size to reduce the influence of the numerical dissipation terms in the turbulent area. The flow structures in the wake of a square cylinder are investigated, especially focusing on the behavior of the separated shear layers.

2. Embedded mesh

The technique of embedded meshes is used over the computational domain $(15d \times 14d \times 4d)$. Figure 2 shows the embedded meshes sliced transversely in the spanwise direction, and the size and the location of each embedded mesh are shown in Table 1.

TABLE 1. Size and Location of Embedded Meshes

	Size	Location of subdomain
inner mesh	91 × 91 × 127	$(-1d, 2d) \times (-1.5d, 1.5d) \times (0, 4d)$
middle mesh	113 × 97 × 57	$(-3d, 4d) \times (-3d, 3d) \times (0, 4d)$
outermost mesh	121 × 114 × 27	$(-5d, 10d) \times (-7d, 7d) \times (0, 4d)$

The inner mesh which surrounds the cylinder is stretched to refine the resolution of the near-wall region of the cylinder. The finest resolution at the cylinder surface is $d/200$ at the front, $d/50$ at the sides and $d/30$ at the rear face, and no-slip velocity boundary conditions are imposed on the surface of the cylinder. The other meshes have uniform grids. The advantage of using embedded meshes is to get high resolution while avoiding the disadvantage of using strongly flattened (anisotropic) grids in LES.

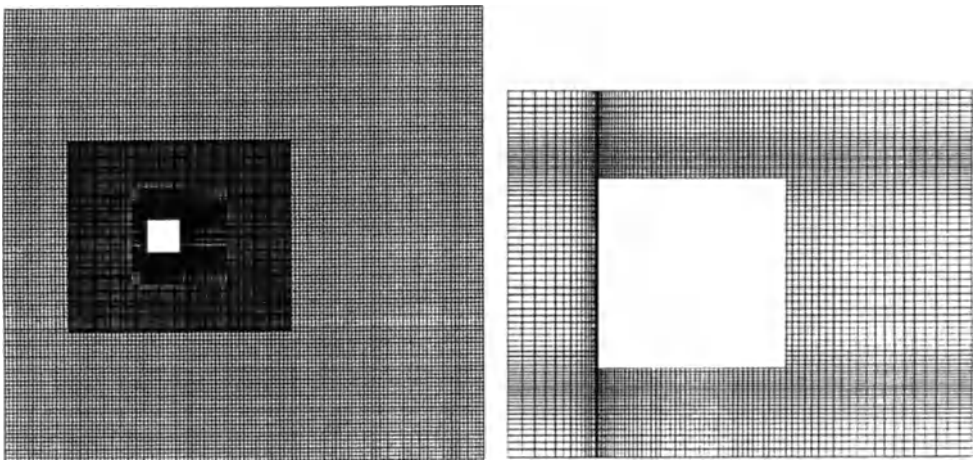

Figure 2. Embedded mesh: left, whole domain; right, vicinity of the square cylinder.

Using embedded meshes, the computed quantities must be exchanged on the interior boundaries. Since we use symmetric Dirichlet condition on the interior boundaries, we have to overlap the computational grids. The Dirichlet boundary condition is calculated using linear interpolation in the overlapped zone. All physical quantities except pressure are exchanged between meshes at every time step. The Poisson equation for pressure is solved by SOR, so we have to exchange pressure data at every iteration.

3. Numerical method

The numerical procedures are based on the MAC method. For the time marching, the first order explicit scheme is used. For discretization, the second-order central spatial differencing is employed except for the convective terms. A non-staggered mesh system is employed, where all physical quantities are defined at the same location for a grid.

In this simulation, the dynamic subgrid-scale model (Germano *et al.* 1991) based on the Smagorinsky model is applied. The coefficient C is evaluated using the least square approach (Lilly, 1992). To stabilize the dynamic model, the coefficient C is bounded to be non-negative but it is not averaged over the spanwise direction.

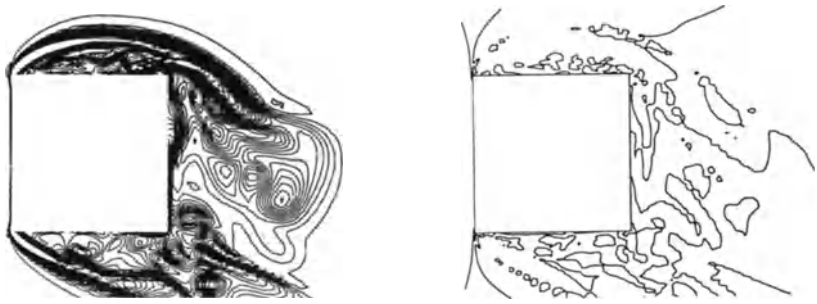

Figure 3. Instantaneous flow pattern around a square cylinder; left, vorticity(ω_z) contours; right, contours of C (contour lines: C=0.01).

4. Computational conditions

The approaching flow is assumed to be uniform(U_0) on the inflow surface boundary and the convective condition is employed on the outflow boundary. The convection velocity is set to be equal to the uniform inflow velocity. Periodic boundary conditions are used in both spanwise and transverse directions. The Reynolds number based on the incoming velocity U_0 and the depth of the square cylinder d is 22,000.

The time step size of this calculation is $0.001(tU_0/B)$ and it cost about 19 hours per shedding cycle on one processor of a Fujitsu VX. Total sampling time is about $39(tU_0/d)$, which is equal to 5 shedding cycles, and the sampling rate of data is about $0.1(tU_0/d)$.

5. Predicted data

Time- and span-averaged values of the reattachment length, Strouhal number, drag coefficient C_d, lift coefficient C_l, rms fluctuation of C_d and rms fluctuation of C_l are give in the preceding paper in this volume by Voke.

Figure 3 shows the instantaneous pattern of vorticity and C around the square cylinder (innermost mesh). The shear flow separating from the front corner of the square cylinder is in the early stage of transition to turbulence and C is estimated below 0.01 in these areas.

References

Germano, M., Piomelli, U., Moin, P. and Cabot, W. H., Phys. Fluids, A3 (1991), 1760.
Kawamura, T. and Kuwahara, K., AIAA-84-0340, (1984).
Lilly, D. K., Phys. Fluids, A4 (1992), 633.

NUMERICAL ANALYSIS OF LES OF FLOW PAST A LONG SQUARE CYLINDER

NORIFUSA KAWASHIMA AND HIROSHI KAWAMURA
Department of Mechanical Engineering,
Science University of Tokyo
Noda-shi, Chiba-ken, 278 Japan

Abstract. The flow past a bluff body is frequently associated with periodic vortex shedding. In this paper, the turbulent flow past a square cylinder is simulated by larg-eddy simulation. The Smagorinsky model (1963) is adopted as the SGS model for the subgrid Reynolds stress term. In addition, an upwind-biased scheme is used for discretizing the convection term to stabilize the numerical calculation. The effect of the upwinding is found to be rather significant. The magnitude of the numerical viscosity term of the upwind scheme is controlled to minimize its effect.

1. Introduction

Most practical engineering flows are turbulent and complex in geometry. Large eddy simulation (LES) provides an effective tool for complex turbulent flows. Subgrid scale (SGS) models are introduced to represent the unresolved subgrid scale motions. The SGS model used most widely is the Smagorinsky model (1963). On the other hand, the dynamic SGS model proposed by Germano *et al.* (1991) has been applied for determining the unknown variable model coefficient from the information of the resolved velocity field.

For the flow past a square cylinder, Mochida *et al.* (1992) simulated the flow using the LES method. A workshop on LES was held coordinated by Rodi and Ferziger in 1995, in which the flow past a square cylinder was one of the cases in the workshop. Several groups submitted the time-averaged and the phase-averaged velocities and turbulent intensities, and compared their results with the experimental data (Lyn *et al.* 1994).

J.-P. Chollet et al. (eds.), Direct and Large-Eddy Simulation II, 413-422.

The Smagorinsky model was applied by Breuer *et al.* ($C_s = 0.1$) and by Kobayashi *et al.* ($C_s = 0.13$), using respectively the 2nd order central and QUICK schemes for the convection term. Wang and Vanka, Archambeau *et al.* and Tamura *et al.* employed the dynamic model, and their calculations were performed with QUICK, the 2nd order central and the 3rd order upwind schemes respectively. The present authors' group calculated the flow using the 3rd order upwind scheme (UTOPIA) for the convection term without the SGS model to investigate the influence of the numerical viscosity on the result.

The main incentive of LES is to perform turbulent simulation with the use of a rather coarse mesh, because if a fine enough mesh could be adopted one could perform a direct numerical simulation. Since it is inevitable to utilize a rather coarse mesh, LES is often associated with problems of numerical instability. A common way to resolve this problem is to introduce an upwind-biased scheme such as QUICK or UTOPIA in the convection term of the momentum equation. The upwind-biased scheme, however, introduces numerical viscosity and contaminates the effect of the SGS model. This is a dilemma in LES work.

In this paper, the turbulent flow past a square cylinder is analyzed by LES using the Smagorinsky model (1963) with the non-slip condition over the solid surface. An upwind-biased scheme is introduced to stabilize the numerical calculation, and an attempt is made to minimize its effect on the numerical results.

2. Fundamental equations

Unsteady incompressible flow is considered. The continuity and grid-filtered Navier-Stokes equations are

$$\frac{\partial \overline{u_i}}{\partial x_i} = 0, \tag{1}$$

$$\frac{\partial \overline{u_i}}{\partial t} + \overline{u_j}\frac{\partial \overline{u_i}}{\partial x_j} = -\frac{1}{\rho}\frac{\partial \overline{P}}{\partial x_i} + \nu\frac{\partial^2 \overline{u_i}}{\partial x_j \partial x_j} - \frac{\partial \tau_{ij}}{\partial x_j}, \tag{2}$$

where

$$\begin{aligned} \tau_{ij} &= \overline{u_i u_j} - \overline{u_i}\,\overline{u_j} \\ &= \underbrace{\overline{\overline{u_i}\,\overline{u_j}} - \overline{u_i}\,\overline{u_j}}_{L_{ij}} + \underbrace{\overline{\overline{u_i}u_j'} + \overline{u_i'\overline{u_j}}}_{C_{ij}} + \underbrace{\overline{u_i'u_j'}}_{R_{ij}}. \end{aligned} \tag{3}$$

We assume that the summation of the Leonard term L_{ij} and the cross term C_{ij} is zero. The standard Smagorinsky model (1963) is adopted as the SGS

model for the Reynolds stress term R_{ij},

$$R_{ij} = \overline{u_i' u_j'} = -2\nu_t \overline{S_{ij}} + \frac{2}{3} K_{SGS} \delta_{ij}, \tag{4}$$

$$\nu_t = (C_s \Delta)^2 (2\overline{S_{ij} S_{ij}})^{\frac{1}{2}}, \tag{5}$$

$$K_{SGS} = \frac{\nu_t^2}{(C_K \Delta)^2}, \tag{6}$$

where K_{SGS} is the subgrid scale turbulent kinetic energy. $\overline{S_{ij}}$ and Δ are the grid scale (GS) strain-rate tensor and the grid-filter width, respectively,

$$\overline{S_{ij}} = \frac{1}{2} \left(\frac{\partial \overline{u_i}}{\partial x_j} + \frac{\partial \overline{u_j}}{\partial x_i} \right) \tag{7}$$

$$\Delta = (\Delta x_1 \Delta x_2 \Delta x_3)^{\frac{1}{3}} . \tag{8}$$

Here, $\Delta x_i (i = 1, 2, 3)$ is the grid spacing in the i direction. In eqs. (5) and (6), the coefficients C_s and C_K are given as

$$C_s = 0.10, \quad C_K = 0.094. \tag{9}$$

To take account of near wall effects, Δ is multiplied by the van Driest wall damping function:

$$f_w = 1 - \exp(-y^+/A^+). \tag{10}$$

The common value adopted for the empirical coefficient A^+ is 26.

3. Calculation methods and conditions

The governing equations are discretized on a staggered grid using the finite difference method. Second order central differencing is adopted for both the pressure and diffusion terms.

The coupling scheme between the continuity and momentum equations is based on the fractional step method. Time marching is performed with use of the 2nd order explicit Adams-Bashforth scheme for both the convection and viscous terms.

The calculation domain is shown in Fig. 1. The number of grids is $109 \times 78 \times 20$ for cases 1 and 2, $125 \times 78 \times 20$ for case 3, and $107 \times 103 \times 20$ for cases 4 and 5. The Reynolds number based on the inflow mean velocity and the square cylinder side length is 22,000. The time increment Δt is 0.0005 for all cases.

The non-slip condition is applied on the surface of the cylinder, while free-slip conditions are adopted on the top and bottom domain boundaries.

TABLE 1. Parameter α

	SGS	Parameter α
case 1	yes	no (2nd order central scheme)
case 2	yes	$\alpha = 1.0$: (whole domain)
case 3	no	$\alpha = 1.0$: (whole domain)
case 4	yes	$\alpha = 1.0$: ($-3.5 \leq y/D \leq 3.5$)
		$\alpha = 0.0$: (otherwise)
case 5	yes	$\alpha = \alpha_0 \exp(-\nu_t/100\nu)$ ($\alpha_0 = 1.0$)

The periodic boundary condition is used in the spanwise direction. At the inflow boundary, constant velocity without perturbation is imposed. For the exit boundary condition, we assume a zero gradient condition for velocity and a constant value for pressure.

Firstly, a calculation has been made using the Smagorinsky model (1963) and with no use of the upwind scheme (case 1). The results, however, suffered from numerical instability. To avoid the numerical instability, the upwind-biased scheme is introduced into the convection term of the Navier-Stokes equation. It is represented by

$$f \left.\frac{\partial \phi}{\partial x}\right|_{x=i} = f_i \frac{-\phi_{i+2} + 8\phi_{i+1} - 8\phi_{i-1} + \phi_{i-2}}{12\Delta x} + \alpha |f_i| \frac{\phi_{i+2} - 4\phi_{i+1} + 6\phi_i - 4\phi_{i-1} + \phi_{i-2}}{12\Delta x}, \quad (11)$$

α is a parameter to control the magnitude of the upwinding. When $\alpha = 0$, it tends to the 4th order central scheme; when $\alpha = 1$, to UTOPIA. The upwind scheme is introduced in the whole region to stabilize the calculation (case 2). On the other hand, the calculation can proceed even without introducing the SGS model (case 3). Thus, the effect of the upwind scheme is quite significant. Then an attempt is made to minimize its effect through control of the magnitude of the parameter α (cases 4 and 5). The model and calculation conditions are summarized in Table 1.

4. Results

An instantaneous velocity field from case 1 is shown in figure 2. Numerical oscillation is observed in the region at the front of the square cylinder. The upwind scheme was introduced for the convection term to prevent occurrence of this numerical instability, as given in Table 1.

The Strouhal number St and the drag coefficient C_D are given in Table 2. The LES calculations (cases 2 to 5) give fairly good agreement with the

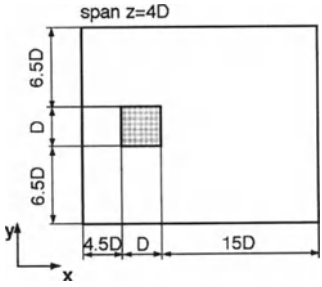

Figure 1. Geometry of the domain.

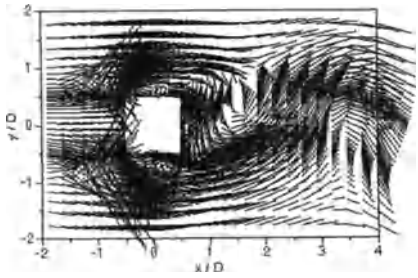

Figure 2. Velocity vectors for case 1.

experimental data (Lyn *et al.* 1994) but are somewhat higher than the experiment.

Figure 3 gives the time averaged streamwise velocity $\overline{u}$ along the vertical line at the center ($x = 0$) of the cylinder top surface. In the following, the overbar and the prime mean the time averaged value on the grid scale and the difference from it, respectively. (Note the different definitions from Eqs.(1) to (4).) In the vicinity of the wall, the calculations underpredict $\overline{u}$ in comparison with the experimental data (Lyn *et al.* 1994). The numerical viscosity in cases 2, 4 and 5 are different, but they do not affect the results in this region much. The cases with the SGS model give a slightly better result. Closer inspection indicates that the reattachment does not take place on the top (or bottom) surface of the cylinder in the experiment while it does in the LES calculations. Moreover a small counterclockwise 'sub-recirculation' is observed in the calculations with the SGS model (cases 2, 4 and 5). These are the reasons for the discrepancies in the present calculations.

Figure 4 shows the distribution of the time averaged streamwise velocity $\overline{u}$ along the centerline. All the calculations underpredict the length of the time averaged separation behind the square cylinder. In front of the square cylinder, the results are not much influenced by the calculation methods, but fairly large differences are found in the wake region. The centerline

TABLE 2. Strouhal number and drag coefficient

	St	C_D		St	C_D
Exp.	0.132	2.1	case 4	0.139	2.73
case 2	0.160	2.72	case 5	0.161	2.78
case 3	0.150	2.65			

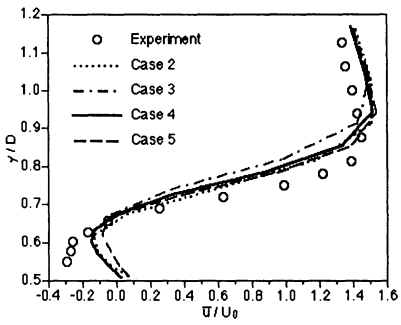

Figure 3. Time-averaged velocity $\overline{u}$ profile at the cylinder center $x = 0$.

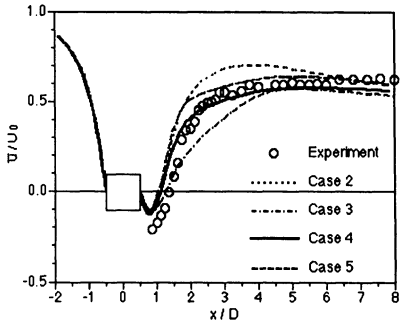

Figure 4. Time-averaged velocity $\overline{u}$ along the centerline $y = 0$.

velocities calculated with the SGS model (cases 2, 4 and 5) approach the free-stream velocity faster than is measured by the experiment (Lyn *et al.* 1994). The centerline velocity of the case 2 (SGS+UTOPIA) first overshoots and then asymptotes to the experimental level. The result of case 3 (UTOPIA only) is lower than the experiment. Among the present calculations, the results with the controlled magnitude of the upwind scheme (cases 4 and 5) give the best agreement with the experiment.

The contours of the mean streamwise velocity $\overline{u}$ are shown in figure 7. The behavior of the calculated results is similar to that of the experimental data. Note that in the region behind the square cylinder, the width of the interval in each contour is different.

Contours of the mean streamwise normal stress $\overline{u'u'}$ are shown in figure 8. Two peaks are observed close to the top and bottom surfaces of the square cylinder, the position and the magnitude of the peak agreeing fairly well with the experimental data. All the calculations give somewhat higher peaks than the experiment.

Contours of the mean crossflow normal stress $\overline{v'v'}$ are shown in figure 9. The position of the maximum point is very close to that of the experiment; however, its peak value is significantly higher than the experimental data. In addition, the fluctuation decays more slowly than the experiment with increasing x. This means that the vertical oscillation of the wake behind the square cylinder is more prominent than that of the experiment.

Figure 10 shows the averaged Reynolds shear stress $\overline{u'v'}$. The peak values of the calculations with the SGS model are higher than those of the experiment. In this respect, the calculation with UTOPIA only (case 3) gives the best agreement with the experiment.

Figure 5 shows contours of the instantaneous ν_t/ν for case 2. The value is low in the vicinity of the cylinder surface. In the region with the periodic

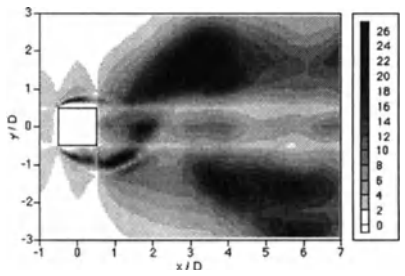

Figure 5. Contours of instantaneous ν_t/ν for case 2

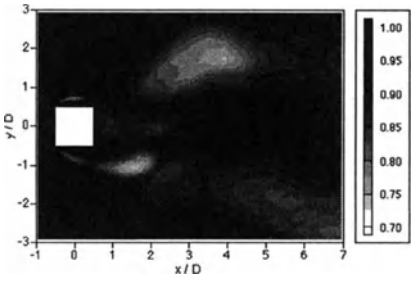

Figure 6. Contours of instantaneous α for case 5

vortex, the magnitude of ν_t/ν is high; in other words, the effect of the SGS model is larger in this region than in the close vicinity of the cylinder.

An attempt has been made to reduce the effect of the upwinding. In case 4, the upwind scheme is introduced only in the central region of the domain, i.e. $-3.5 \leq y/D \leq 3.5$; if the region of nonzero α is restricted further, the numerical calculation becomes unstable. In case 5, the magnitude of parameter α is decreased as a function of ν_t/ν as given in Table 1. Though the parameter α is not uniform in cases 4 and 5 (see Figure 6), the calculations proceed stably and their results are in better agreement with the experiment. A refinement of the method to control α is left for further investigation.

5. Conclusions

The turbulent flow past a square cylinder has been calculated by LES using the Smagorinsky model. Because of a rather coarse mesh, which is unavoidable in LES, numerical instability was observed in the front region of the cylinder. To avoid the instability, an upwind-biased scheme (UTOPIA) was introduced in the whole calculation region; however, its effect on the calculated flow field was rather significant. Thus an effort was made to reduce the region in which the upwind scheme is introduced. The calculation was numerically stable and an improvement was obtained compared with LES using the upwind scheme in the whole region.

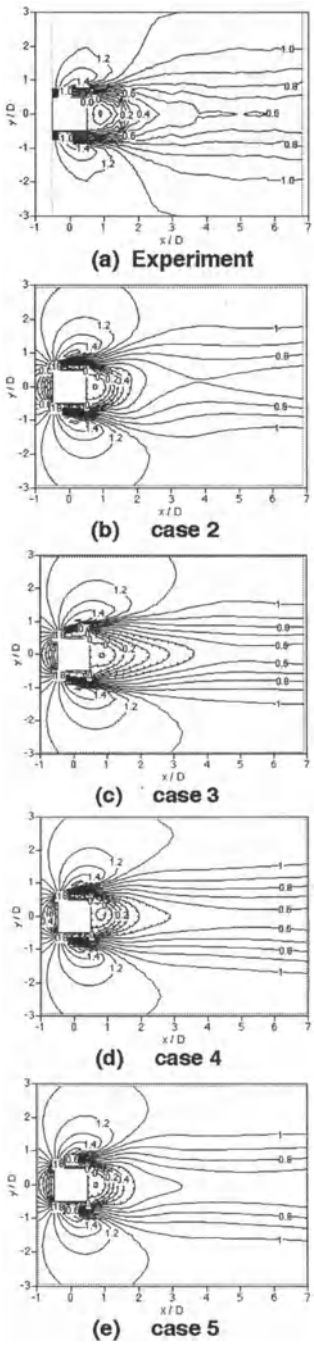

Figure 7. Time-averaged velocity $\overline{u}$.

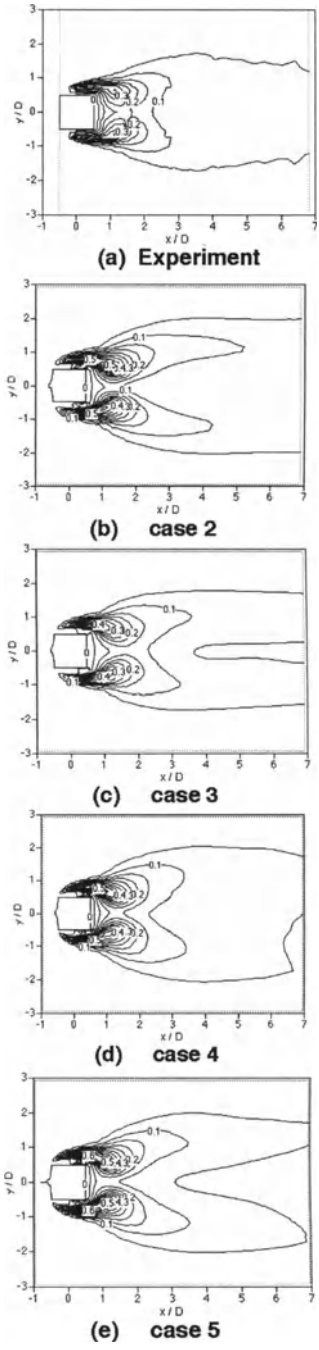

Figure 8. Time-averaged stress $\overline{u'u'}$.

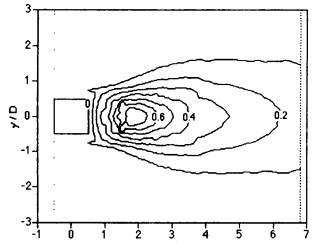

(a) Experiment

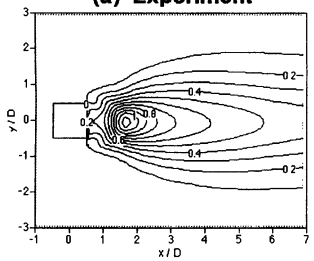

(b) case 2

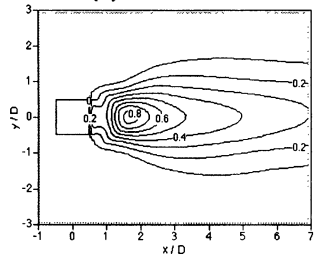

(c) case 3

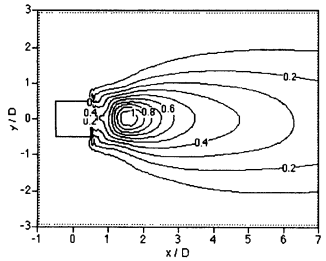

(d) case 4

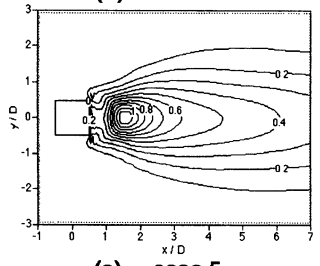

(e) case 5

Figure 9. Time-averaged stress $\overline{v'v'}$

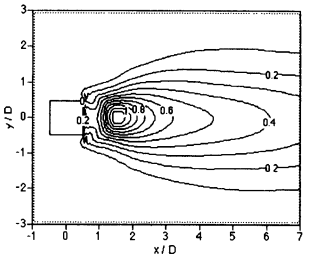

(e) case 5

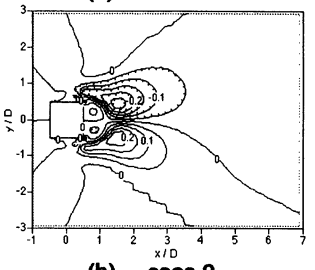

(b) case 2

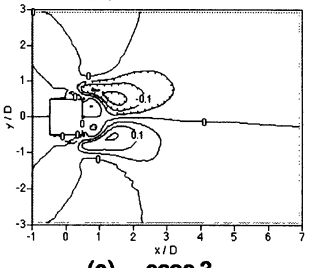

(c) case 3

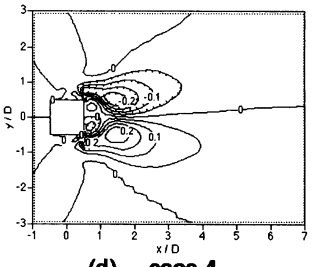

(d) case 4

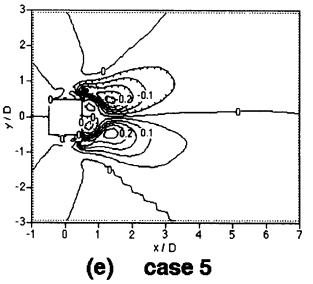

(e) case 5

Figure 10. Time-averaged stress $\overline{u'v'}$

References

Archambeau, F., Laurence, D. and Leschziner M. A., (1995) Test case A: Vortex Shedding behind a Square Prism at $Re = 21,400$, *Workshop on Large Eddy Simulation of Flows past Bluff Bodies*, Rottach-Egern, Germany.

Breuer, M., Pourquie, M. and Rodi, W., (1995) Description of the LES Method for the Workshop on Large Eddy Simulation of Flows past Bluff Bodies, *Workshop (ibid.)*.

Germano, M., Piomelli, U., Moin, P. and Cabot, W. H. (1991) A Dynamic Subgrid-scale Eddy Viscosity Model, *Phys. Fluids*, A**3**, pp 1760–1765.

Kawamura, H. and Kawashima, N., (1995) Vortex Shedding past a Square Cylinder, *Workshop (ibid.)*.

Kobayashi, T., Taniguchi, N. and Kogaki, T., (1995) Description of Numerical Methods, Boundary Conditions and SGS Models for Workshop on Large Eddy Simulation of Flow past Bluff Bodies *Workshop (ibid.)*.

Lyn, D. A., Einav, S., Rodi, W. and Park, J. H. (1994) A Laser-Doppler Velocimetry Study of Ensemble-Averaged Characteristics of the Turbulent near Wake of a Square Cylinder, Rept. SFB 210/E/100.

Mochida, A., Murakami, S., Rodi, W. and Sakamoto, S., (1992) Comparison of LES with DSM, $k - \varepsilon$ and Experiments for Turbulent Vortex Shedding Flow past 2D Square Cylinder, *Proc. 6th Symp. on Computational Fluid Dynamics (in Japanese)*, pp 277–280.

Smagorinsky, J. (1963) General Circulation Experiments with the Primitive Equations. Part I. the Basic Experiment, *Monthly Weather Review*, **91**, pp 99–164.

Tamura, T., Takakuwa, A. and Nozawa, K., (1995) Test case A: Vortex Shedding past a Square Cylinder, *Workshop (ibid.)*.

Wang, G. and Vanka S. P., (1995) Description of Large Eddy Simulation of Flow past a Square Cylinder, *Workshop (ibid.)*.